



European Research Infrastructure supporting Smart Grid Systems Technology Development, Validation and Roll Out

Technical Report TA User Project

Sundom Hardware-In-the Loop Living Lab

Grant Agreement No:	654113
Funding Instrument:	Research and Innovation Actions (RIA) – Integrating Activity (IA)
Funded under:	INFRAIA-1-2014/2015: Integrating and opening existing national and regional research infrastructures of European interest
Starting date of project:	30.7.2018
Project Duration:	7 weeks

Contractual delivery date:	4.2.2019
Actual delivery date:	4.2.2019
Name of lead beneficiary for this deliverable:	Kimmo Kauhaniemi, University of Vaasa, Finland
Deliverable Type:	Report (R)
Security Class:	Public (PU)
Revision / Status:	For Review

Document Information

Document Version: 1.0
 Revision / Status: For Review

All Authors/Partners

Katja Sirviö, University of Vaasa, Finland
 Mike Mekkanen, University of Vaasa, Finland
 Kimmo Kauhaniemi, University of Vaasa, Finland
 Davood Babazadeh, OFFIS, Germany

Distribution List

University of Vaasa
 OFFIS

Document History

Revision	Content / Changes	Resp. Partner	Date
1.0	Draft	UVA / Sirviö	5.12.2018
1.0	For Review	UVA / Sirviö, Mekkanen	7.1.2019

Document Approval

Final Approval	Name	Resp. Partner	Date
[Review Task Level]	[Given Name + Name]	[Partner Short Name]	DD.MM.YY
[Review WP Level]	[Given Name + Name]	[Partner Short Name]	DD.MM.YY
[Review Steering Com. Level]	[Given Name + Name]	[Partner Short Name]	DD.MM.YY

Disclaimer

This document contains material, which is copyrighted by certain ERIGrid consortium parties and may not be reproduced or copied without permission. The information contained in this document is the proprietary confidential information of certain ERIGrid consortium parties and may not be disclosed except in accordance with the consortium agreement.

The commercial use of any information in this document may require a licence from the proprietor of that information.

Neither the ERIGrid consortium as a whole, nor any single party within the ERIGrid consortium warrant that the information contained in this document is capable of use, nor that the use of such information is free from risk. Neither the ERIGrid consortium as a whole, nor any single party within the ERIGrid consortium accepts any liability for loss or damage suffered by any person using the information.

This document does not represent the opinion of the European Community, and the European Community is not responsible for any use that might be made of its content.

Copyright Notice

© The ERIGrid Consortium, 2015 – 2020

Table of contents

Executive Summary	6
1 General Information of the User Project.....	7
2 Research Motivation	9
2.1 Objectives	10
2.2 Scope.....	12
3 State-of-the-Art/State-of-Technology	15
4 Executed Tests and Experiments	18
4.1 Test Plan.....	19
4.2 Standards, Procedures, and Methodology.....	20
4.3 Test Set-up.....	23
4.4 Data Management and Processing.....	23
5 Results and Conclusions	24
5.1 Developed use cases by Simscape Power Systems	24
5.1.1 Scenario 2018/1 – Situation 2018.....	24
5.1.2 Scenario 2018/2 – RPW control	28
5.1.3 Scenario 2028/1.....	28
5.1.4 Scenario 2028/2 – SR.....	30
5.1.5 Scenario 2028/3 – SR and $\cos \varphi$ control of PV inverters	31
5.1.6 Scenario 2028/4 – SR and RPW control of WT converter	31
5.1.7 Scenario 2028/5 – SR and RPW+NDZ control of WT converter	31
5.1.8 Scenario 2028/6 – SR, RPW control of WT converter and $\cos \varphi$ control of PV inverters	32
5.1.9 Scenario 2028/7 – SR, RPW+NDZ control of WT converter and $\cos \varphi$ control of PV inverters	32
5.1.10 Scenario 2028/8 – SR and RPW+NDZ control of PV inverters.....	32
5.1.11 Scenario 2028/9 – SR, RPW control of WT converter and RPW+NDZ control of PV inverters	34
5.1.12 Scenario 2028/10 – SR, RPW+NDZ control of WT converter and RPW+NDZ control of PV inverters	34
5.1.13 Scenario 2035/0.....	35
5.1.14 Scenario 2035/1 – SR.....	35
5.1.15 Scenario 2035/2 – SR and $\cos \varphi$ control of PV inverters	36
5.1.16 Scenario 2035/3 – SR and RPW+NDZ control of WT converter	36
5.1.17 Scenario 2035/4 – SR, RPW+NDZ control of WT converter and $\cos \varphi$ control of PV inverters	36
5.1.18 Scenario 2035/5 – SR and RPW+NDZ control of PV inverters.....	37
5.1.19 Scenario 2035/6 – SR, RPW+NDZ control of WT converter and RPW+NDZ control of PV inverters	37
5.1.20 Scenario 2035/7 – RPW+NDZ control of PV inverters.....	38
5.1.21 Scenario 2035/8 – RPW+NDZ control of WT converter and RPW+NDZ control of PV inverters	38
5.2 Offline simulations by RT-lab.....	39
5.2.1 Scenario 2018/1.....	39
5.2.2 Scenario 2018/2.....	41
5.2.3 Scenario 2028/1.....	43
5.2.4 Scenario 2028/2 – SR.....	44
5.2.5 Scenario 2028/3 – SR and $\cos \varphi$ control of PV inverters	44
5.2.6 Scenario 2028/4 – SR and RPW control of WT converter	44
5.3 Real-time simulations	47
5.3.1 Software in the loop simulations	47
5.3.2 Controller hardware in the loop simulations	51
5.3.3 The round trip Goose latency	56
5.3.4 Comparison of the different simulations	58

6 Open Issues and Suggestions for Improvements 61

7 Dissemination Planning 62

8 References 63

9 Annex 64

 9.1 List of Figures 64

 9.2 List of Tables 67

Abbreviations

<i>AS</i>	Ancillary Services
<i>CHIL</i>	Controller Hardware In the Loop
<i>DER</i>	Distributed Energy Resource
<i>DMS</i>	Distribution Management System
<i>DR</i>	Demand Response
<i>HEMS</i>	Home Energy Management System
<i>MGCC</i>	Microgrid Central Controller
<i>RPW</i>	Reactive Power Window
<i>SIL</i>	Software In the Loop
<i>SR</i>	Shunt Reactor
<i>SSG</i>	Sundom Smart Grid
<i>TA</i>	Trans-national Access
<i>WT</i>	Wind Turbine

Executive Summary

The aim of this research was to build up a real-time co-simulation platform for a sub-urban area, Sundom Smart Grid (SSG) in Vaasa, Finland. The case studies performed with the developed platform were related to technical ancillary services (AS), particularly to reactive power control provided by distributed energy resources (DER), connected to medium voltage (MV) and low voltage (LV) distribution networks.

The developed real time co-simulation platform is based on OPAL-RT's real-time simulation system OP5600, consisting of power system simulations with ePhasorsim (frequency domain/phasor or RMS type), control and communications simulations with eMegasim (time domain/EMT or discrete type). More specifically, ePhasorsim is a block presenting the electric power grid behaviour in phasor mode in the eMegasim platform. eMegasim runs on the RT-LAB real-time simulation platform, which is OPAL-RT's real-time simulation software, fully integrated with MATLAB/Simulink. The communication between controllers and simulated power system interfaces was implemented by IEC61850 Goose on Ethernet.

Three base network scenarios were selected to be developed further for AS studies, namely Status 2018, Scenario 2028 and Scenario 2035. First, these base scenarios of the power grid were modelled with Powerfactory software, where the load and generation data, as well as the voltage in the HV side were defined based on the results of earlier simulations with Simscape Powersystems. These initial values were essential for running the power flow calculations in Powerfactory, in order to determine the initial status of the network. The results of the power flow calculations were migrated into an Excel file, the aim of which was to represent the power grid in the certain initial status within the ePhasorsim block. In order for the generated ePhasorsim block to interact with the control system, the inputs and outputs were defined also in the generated Excel file.

The developed reactive power window (RPW) control algorithm was implemented as a controller for the MV connected 3.6. MW wind turbine (WT) converter to control reactive power flow at the HV/MV connection point of the simulated power system. The behaviour of the controller was studied both as a software-in-the-loop (SIL) and as a controller-hardware-in-the-loop (CHIL) in several different network scenarios.

The outcome of the research work is a number of scientific papers from the developed test platform, framework and control schemes for future AS that LV microgrids could offer in developing sub-urban areas, as in the case example of SSG. Further, the developed use cases and framework, as well as the developed test bed for them, could be utilized in future research projects as well as improve the co-operation between academia and industry. Future studies could consist of different microgrid control strategies during utility grid connected operation. In other words, the developed test bed offers a flexibility platform to enable the operation of microgrid flexible resources in different technical service markets.

1 General Information of the User Project

The project title is Sundom Hardware in the Loop Living Lab and the acronym is SunHILL. The access period was 30.7.2018 – 14.9.2018. The user group members were professor Kimmo Kauhaniemi, PhD student Katja Sirviö and assistant professor Mike Mekkanen. In the following paragraphs the members of the proposing team are presented in more detail.

Katja H. Sirviö was born in Vaasa, Finland, in 1973. She received a B.Sc. degree in electrical engineering from VAMK Ltd, University of Applied Sciences, Vaasa, in 1998 and a M.Sc. degree in electrical engineering from the University of Vaasa, in 2012. She is currently pursuing a Ph.D. in electrical engineering at the University of Vaasa. Katja worked previously as an entrepreneur and managing director in the electrical planning and installations (KHS-Sähkö Ltd) sector, and thereafter she was a R&D project manager at ABB Ltd Low Voltage Products. Presently she is employed by the University of Vaasa as laboratory engineer and is currently leave-of-absence for the completion of her doctoral studies. Her research interests include the evolution, development and management of future low voltage distribution networks.

Mike Mekkanen received a B.Sc. degree in electrical engineering at the University of Technology, and his M.Sc. and Ph.D. degrees in Industrial Automation from the University of Vaasa, in 2010 and 2015 respectively. Currently he is assistant professor of the School of Technology University of Vaasa. Prior to joining University of Vaasa, he worked in different positions and worldwide companies, for instance Mandor Co Iraq, Eagle Co, The Ministry of Defence and The Ministry of Higher Education, Libya, where he directed a diverse program that included systems level design, as well as test and implementation in electrical networks. At the University of Vaasa he has established a DEMVE laboratory and training program. His special interest areas include Smart Grid, Digital SAS, FPGA, embedded systems and communication systems.

Kimmo T. Kauhaniemi received his M.Sc. degree in 1987 and his Ph.D. in 1993 in electrical engineering from Tampere University of Technology, Finland. He has been employed by ABB Corporate Research, and VTT Technical Research Centre of Finland. Currently he is with the University of Vaasa, where he is Professor of Electrical Engineering. His special interest areas include power system transient simulation, protection of power systems, grid integration of distributed generation, and microgrids.

Related research according to SunHILL has been the project “Sundom Smart Grid” – This was a joint project at the City of Vaasa in cooperation with ABB, a local telecom company Anvia (now part of Elisa) and the local electric utility Vaasan Sähköverkko. The project was coordinated by Merinova Oy. In this project, a unique Smart Grid pilot was established in a real MV network. ABB equipped the primary substation and four secondary substations with modern IEDS, while Anvia provided fibre optic connections for each IED and set up a cloud service to collect the IEC 61850 based measurements from the network. A direct communication link from the site to the University’s laboratory was also set up. The project was finalized by the end of 2015, but the data collection facilities have been used since then in various research activities.

A second related study has been done in “SESP – Smart Energy System Platform” project, the aim of which is to build a new smart energy systems research platform, which will form part of the Vaasa Energy Business and Innovation Center (VEBIC). This platform consists of a laboratory environment, which will be located at VEBIC; living lab sites and business models, which are defined jointly with the collaborating industry; and a big data warehouse, which will be established in this project and sustained by VEBIC.

The third related project is “DeCAS – Demonstration of coordinated ancillary services” covering study and demonstration of ancillary services covering different voltage levels and integration to the future markets. DeCAS is ERA-Net SmartGrid+ funded project including partners of four European countries. The aim of the project is to build up DeCAS Innovation Cells on three existing demonstration

sites whose current state will be utilised and the developed solutions will be transferred and validated. Focus of the project is to research and analyse system services such as demand response and coordination of individual Volt/Var control concepts over high voltage level through low voltage level in consideration of respective market integration concepts.

2 Research Motivation

The standardization of microgrid controllers is still in its development phase. The status of IEEE and IEC standards is listed in Table 1 and it can be seen that the majority of them are in development progress. The impact of standardization for product development can be presented as a general cycle of product sales and standardization, which is presented in Figure 1. Based on the state of the standardization it can be concluded that microgrid controllers are in the phase “need to resolve issues related to product standards”. Therefore, it is essential to build up a comprehensive test platform for microgrid controllers that can perform the simulations (CHIL) and tests of different types of required functionalities [1], [2] of microgrid controllers. In addition, the test platform should be flexible so that it can be transformed into different kinds of microgrids.

Table 1. State of the microgrid controller in IEEE and IEC standardization.

Code	Status	Date	Name
IEC TS 62898-1	Published	May 2017	Microgrids - Part 1: Guidelines for microgrid projects planning and specification
IEC TS 62898-2	Active Project		Microgrids - Guidelines for Operation (and Control)
IEC TS 62898-3-1	Active Project		Microgrids - Technical Requirements - Protection
IEEE P1547-2008 series	Approved, rev. 2003	Feb 2018	Interconnection and Interoperability of Distributed Energy Resources with Associated Electric Power Systems Interfaces
IEEE 2030.7	Approved Draft	Jan 2018	Specification of Microgrid Controllers
IEEE P2030.8	Unapproved Draft	Mar 2018	Standard for the Testing of Microgrid Controllers
IEEE P2030.9	Active Project		Recommended Practice for the Planning and Design of the Microgrid
IEEE P2030.10	Active Project		Standard for DC Microgrids for Rural and Remote Electricity Access Applications

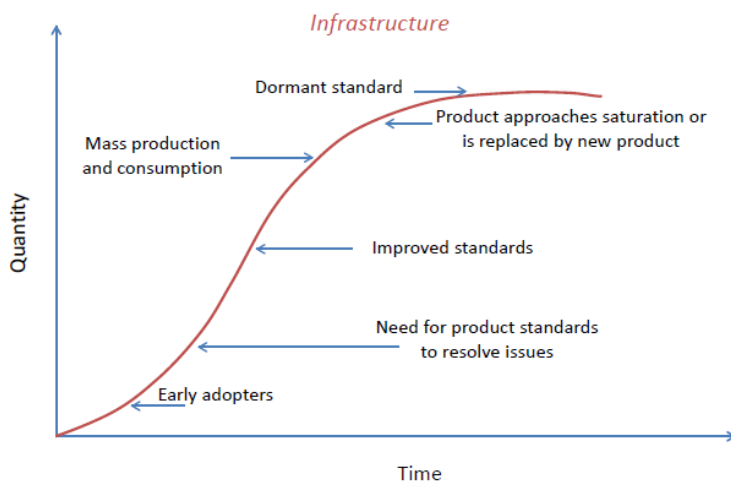


Figure 1. Product sales and standards cycle.

Options for ancillary services are one main focus on the development of Smart Grids and microgrids, which is a result but also a possibility due to massive implementation of distributed generation (DG) units. Sundom Smart Grid, Innovation Cell Finland in DeCAS project, enables the development of ancillary service solutions for future grids over traditional boundaries from the high voltage level until to the LV level. SSG is a pilot living lab jointly created by ABB, Vaasan Sähköverkko (DSO), Elisa (communications) and University of Vaasa. The overview of the system is presented in Figure 2. Real-time measurements are gathered from the MV distribution network on-line, from all four feeders at a HV/MV substation as well as from three MV/LV substations comprising 20 measurement points totally. The measured data is IEC 61850 stream with current and voltage measurements. The sampling rate is 80 samples per a cycle, which is 4000 samples/s. In addition power, frequency, RMS voltages, currents etc. measurements are received by GOOSE messages. The data is collected to servers for providing data also for future research.

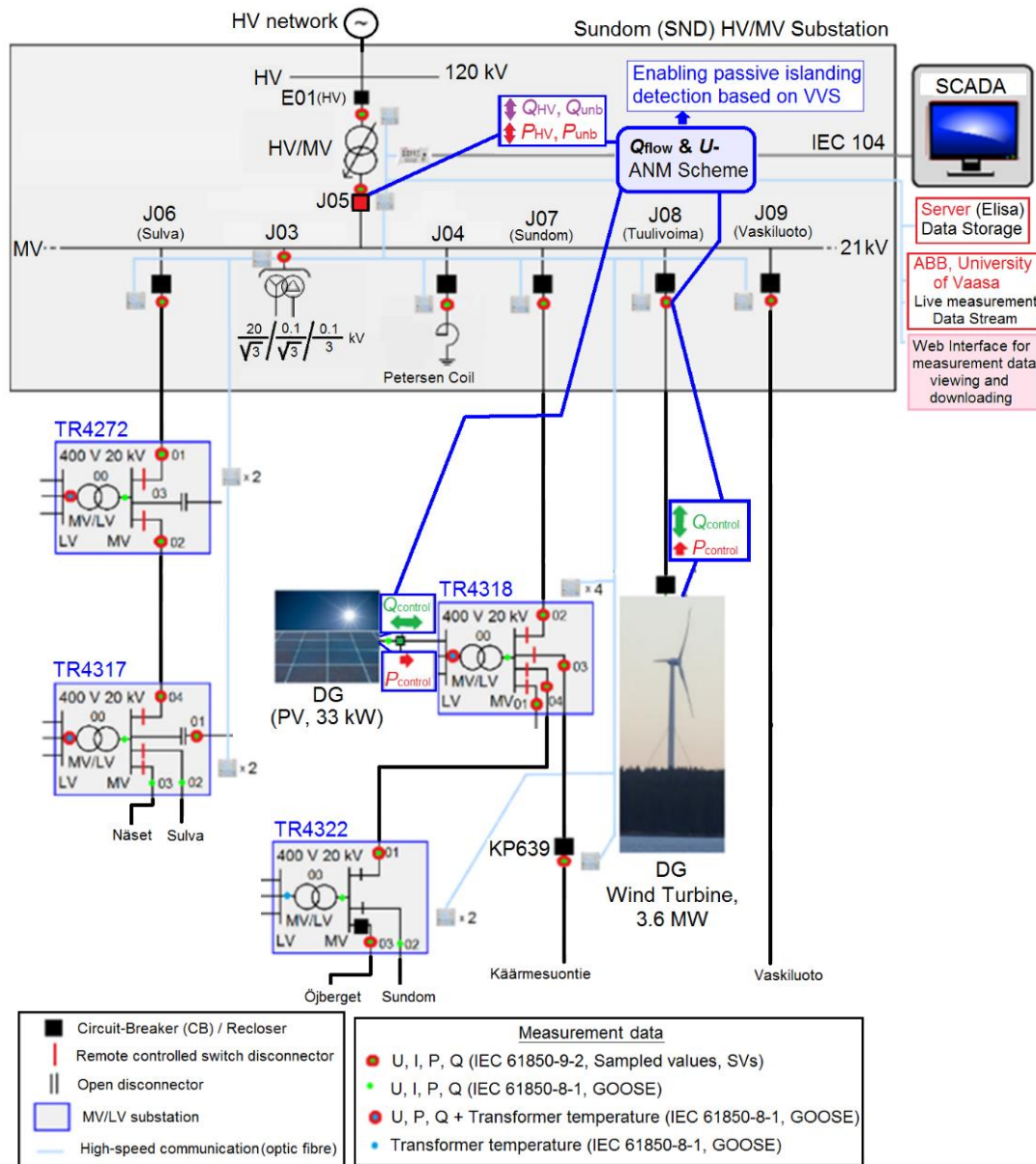


Figure 2. On-line diagram of Sundom Smart Grid living lab.

2.1 Objectives

The aim of this research was to study and develop a real-time co-simulation platform integrating real measurement data stream from SSG, a simulated power grid, communications, control functions, CHIL and a communications emulator for the future microgrid studies. The benefit of this developed platform could be realized by different use cases e.g. for demand response (DR) and technical AS actions for the sub-urban area, living lab SSG.

The first objective was to build up real-time simulation models or ePhasorsim models for developing the SSG power grid. For the real-time co-simulations in the eMegasim platform the interfacing (inputs and outputs) of the generated ePhasorsim block was developed. At present, this interfacing is available for PSS/E, PowerFactory, and the Excel type of power system simulation models. In this study, the Excel was utilized. After the developed power grid model, the aim was to develop real-time models representing the functionalities or control algorithms of the microgrid central controller (MGCC),

the distribution management system (DMS), for the studied use cases. Then the aim was to integrate the ePhasorsim block and tune the developed controllers in eMegasim to operate correctly in real-time. Further, the idea was to integrate IEC61850 Goose communication to the developed models. Finally the generated RPW algorithm was to be implemented to hardware and run the simulations as CHIL.

The research and development work had following phases:

- 1) Determination of requirements for the simulation platform based on the developed use cases
- 2) Model development
 - a) Modelling the SSG scenarios (Situation 2018, Scenario 2028, and Scenario 2035) in Powerfactory
 - b) Defining initial values from Simscape Powersystem simulations for power flow calculations in Powerfactory
 - c) Migrating the results of the power flow calculations into Excel files
 - d) Defining the inputs and outputs of the ePhasorsim blocks in the Excel files
 - e) Implementing input data, measurements, controllers and ePhasorsim blocks in eMegasim platform
 - f) Implementing IEC61850 GOOSE communications in eMegasim
- 2) SIL simulation cases run
- 3) Platform preparation
 - a) Programming of hardware controller
 - b) Interface testing, GOOSE
 - c) RT power system model adaptation into CHIL simulations
 - d) Test case run
- 4) CHIL simulation cases run

The operational scenarios were developed for technical AS, reactive power control, in SSG. The developed simulation models include developing distribution network as described below.

- 1) Situation 2018
 - MV distribution network model (background network, primary transformer 117/21 kV, feeders, cables, overhead lines, load data, secondary transformers)
 - LV distribution network model (secondary transformers, load data)
 - WT 3.6 MW with a full scale converter at MV feeder (generation data)
 - Inverter connected PV 33.6 kWp at LV distribution network (generation data)
- 2) Scenario 2028:
 - Models as in the previous phase
 - Increased amount of PV up to 25 % of the customers (2.6 MWp in total)
 - Load increase
 - Increased cabling degree
- 3) Scenario 2035
 - Models as in the previous phase
 - Increased amount of PV up to 50 % of the customers (5.3 MWp in total)
 - Load increase

2.2 Scope

At present there exists as well as for future microgrids there is coming different requirements for reactive power flow. EU sets grid code requirements, for example, for connection of demand and generators [3], [4]. Further local TSO set requirements for active power flow dependent reactive power flow (P_{flow} and Q_{flow}) by “Reactive Power Window” [5]. In addition, reliable and future-proof islanding detection as well as possibility to make stable transition to islanded operation sets requirements for reactive power flow control [6], [7], [8], and [9]. In Figure 3 is presented the different requirements for reactive power flow in case SSG. In this project, Fingrid’s reactive power window (RPW) was considered for reactive power management by the different use cases. The developed RPW control algorithm in [10] was utilised for the case studies and simulation scenarios.

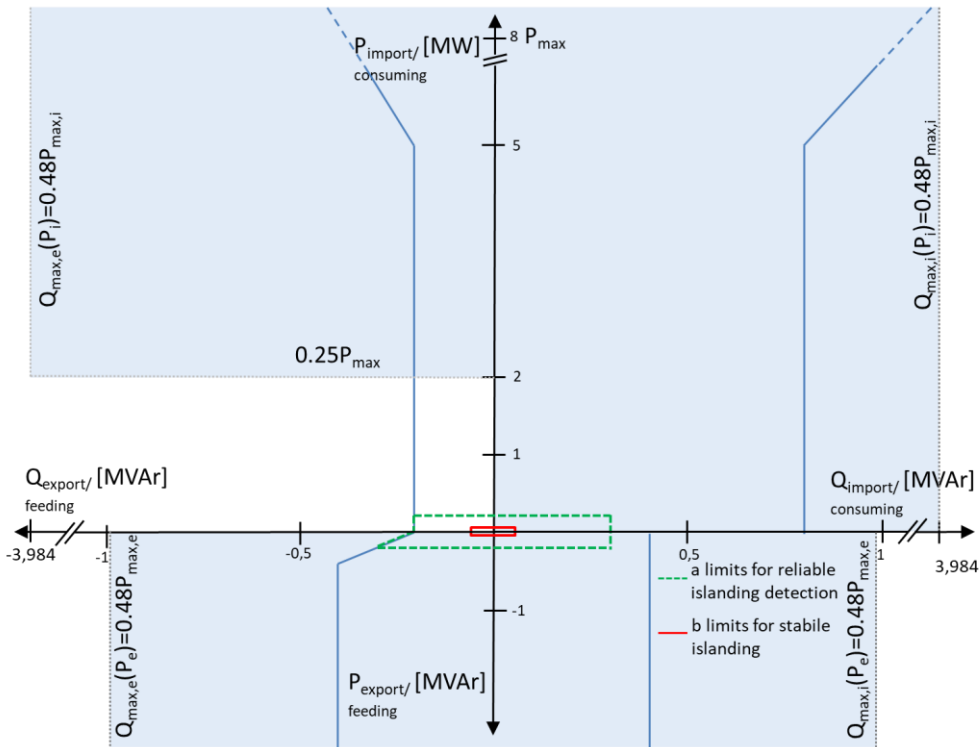


Figure 3. On-line diagram of Sundom Smart Grid living lab. [10]

The real-time simulation platform was constructed for studies such as reactive power control for technical AS, but it could be utilized also further for DR studies. The evaluation of control strategies for the AS of a microgrid controller was in the main focus of the developed scenarios. The scenarios showed the effect and the influence of MV and LV connected DER control in multi-time domain. The reactive power at the HV/MV connection point was controlled through the full-scale converter of the 3.6 MW WT, which is solely connected to an MV feeder. The information exchange between simulated system and SIL or CHIL for AS is presented in Figure 4.

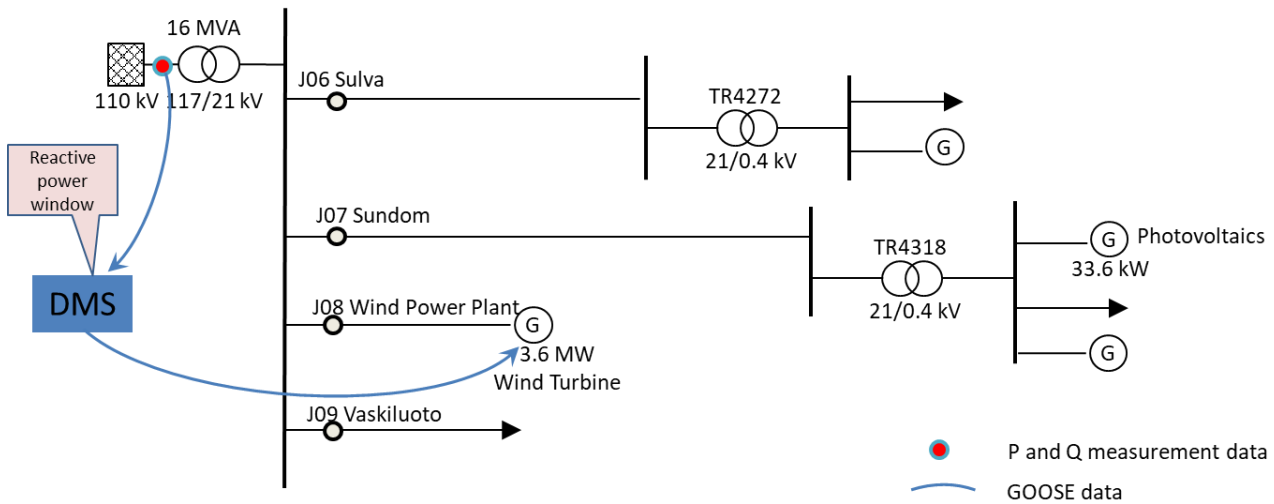


Figure 4. The outline of the simulated network.

The simulation architecture is based on the RT-Lab platform, which manages the projects and real-time models, compiles the models, loads them to the OP5600 real-time simulator and manages the real-time simulation runs. The real-time simulation models were developed with Matlab/Simulink R2013a. For a complete real-time model there are two basic building blocks namely SC_modelname and SM_modelname interlinked together. SM_ is for the calculations in OP5600, and SC_ is for GUI in PC, where one can manage the controllable parameters during a real-time simulation run. In Figure 5 is illustrated the simulation architecture in the SM_block for SIL of reactive power control in SSG Status 2018.

One outcome is a MV distribution network / microgrid simulation model and showcase with different time domains connected to the SSG. The developed real-time co-simulation platform could be utilized further for academic research as well as electrical industry. In Vaasa there is over 140 companies in energy business or industry sector. This offers excellent basis for future research of different type of Smart Grid control scenarios, and also to test and verify, for example, standardized microgrid control functionalities like demand response and different ancillary services and also to develop new and better ones for the future. In addition the platform enables analysis of the IEC 61850 standard and functionalities based on it.

Further, this platform will aid designing and establishing the communication architecture to exchange data between selected sites, DMS and real-time simulation system for these kind of co-simulation platforms. Finally, target is to integrate this "Future Living Lab" with the existing PAC laboratory at the University of Vaasa by using a hybrid system which consists of IEC 61850 communication (also wireless 5G in the future), IP based network and IEEE 802.15.4 WSN opens new research possibilities to study also different Smart Grid communication aspects.

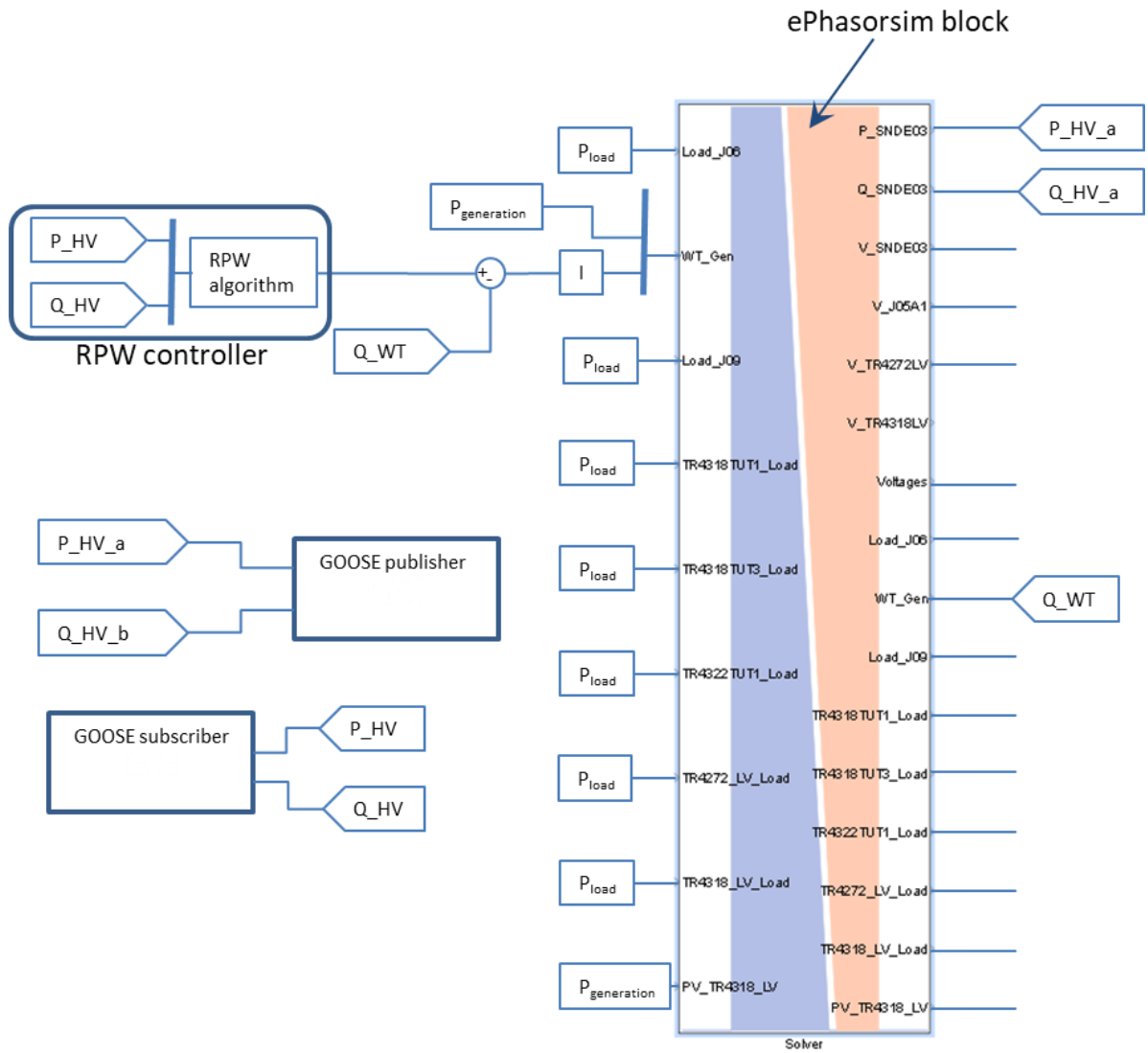


Figure 5. The simulation architecture in SM_block for SIL of reactive power control in SSG Status 2018.

3 State-of-the-Art/State-of-Technology

Future power systems will be complex systems to model because of the integrated renewable technologies includes power electronic interfaces and because of the increased use of smart technologies of power systems. Power-flow and transient stability tools cannot always model details with the precision needed, sometimes even some network elements are impossible to model. Therefore, they are inadequate separately for representing all relevant characteristics of complex networks. In turn, electromagnetic transient (EMT) tools provide detailed and accurate results but run slowly so a complete network cannot be modelled. [11]

Today most of the simulations are offline simulations with PCs. In addition, it is possible to use RT simulators for example controller testing (EMT simulations) as hardware in the loop (HIL) or controller in the loop (CHIL). The past, present and future of simulations are presented in Figure 6, where cyber physical energy systems (CPES) aspects are presented in the upper and co-simulation system features in the lower section. Currently there is a lack of methods and tools for combining these aspects, but highly specialized methods and tools for different individual domains exist [12].

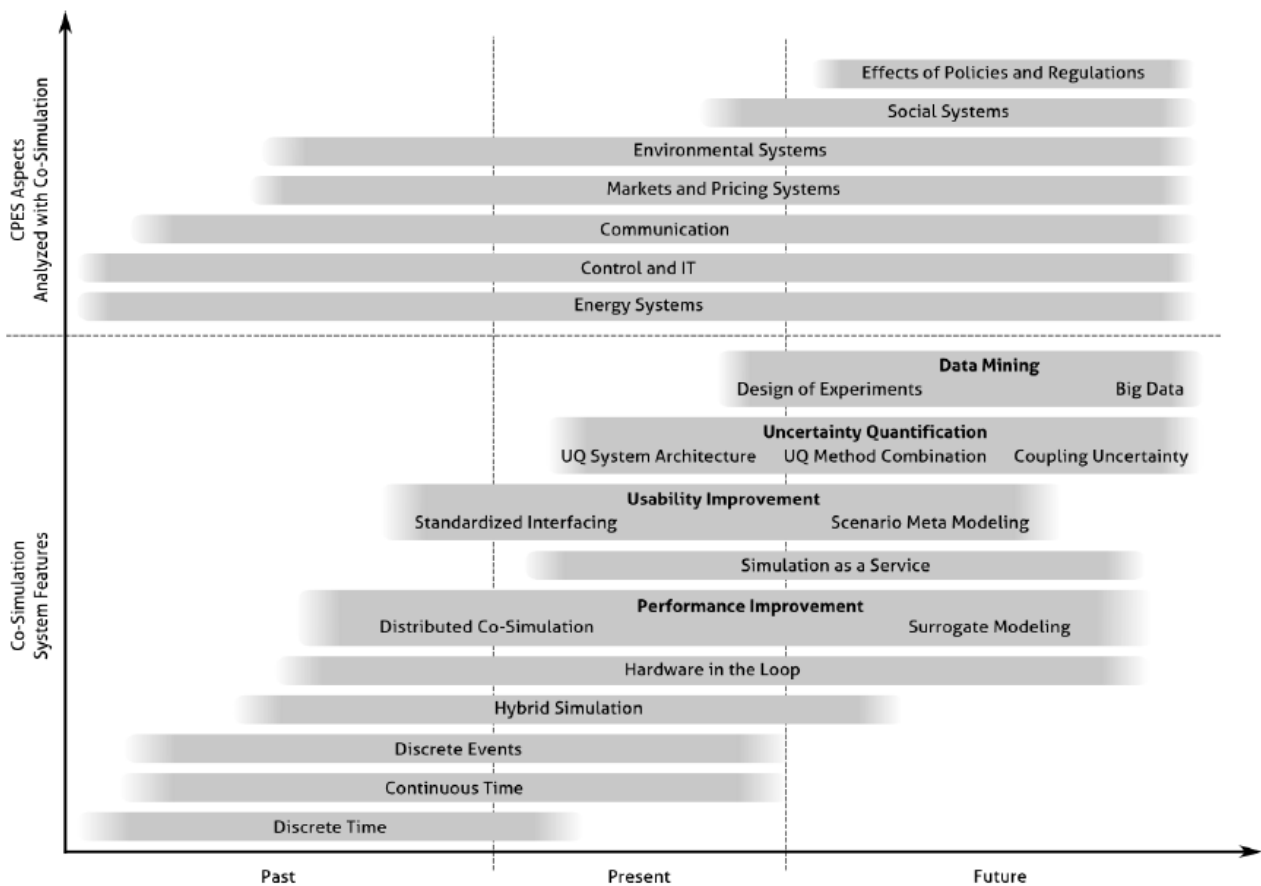


Figure 6. The past, present and future of simulations. [13]

Coupling between continuous simulation of power systems and discrete event based simulation (e.g. communication) or coupling between time and frequency domain simulations are very topical issues for Smart Grid and Microgrid studies at present. In addition combining the simulations to automation systems or control devices/systems are in great interest. The following four types of techniques are introduced by [6] for simulating domain specific models: classic simulations, parallel simulations, hybrid simulations and co-simulations. In classic simulations, a model is run within a dedicated runtime environment/solver. Running simulations in parallel on multiple solvers speeds up the runtime. Different types of representations are integrated into one single runtime environment in

hybrid simulations. In co-simulations a complex setup of different types of are executed or solved in individual runtime environments. Further when approaching RT co-simulations by combining different types of simulations for generating a hybrid simulation model (power system, ICT ...), the different representations has to be synchronized to run in universal time. In RT co-simulation offline simulations are run within RT constrains together hardware in the loop (HIL) or power hardware in the loop (PHIL) and RT simulated model. [15]

So far, different control and management functionalities of microgrids have been simulated and tested [8]. Pilot cases for different type of microgrids have emerged with early stage microgrid controllers. Some standards for microgrids have been published, but the standardization of microgrid controllers is still under development. The standardization of microgrid controllers is intended to define the requirements for microgrids “regardless of topology, configuration or jurisdiction and to present the control approaches required from the distribution system operator and the microgrid operator [1]”. In addition, transmission system operator and distribution system operator set requirements for network operation, which are taken in account when developing and testing microgrid operation and controller functions. These requirements can relate to the technical AS for example voltage/reactive power (U/Q) control.

Testing of the microgrid controllers is very topical issue today. The test program functional requirements should embody the functional use cases for microgrids. The functional requirements are frequency control, voltage control, intentional transition to island operation, unintentional transition to island operation, resynchronization and reconnection, energy management in grid connected as well as in island operation, protection, ancillary services, black start and microgrid user interface and data management [9]. The evaluation of microgrid controller performance can be performed with different test setups, which can be pure simulation, CIL, CHIL and PHIL, and hardware only [18]. Pure simulation is utilized in very early stage of product development. In CHIL simulation the controller is a real device, but everything else is simulated. In PHIL simulations there are real power devices (e.g. PV unit) in addition to the controller [18].

Telecommunication (like wireless high-speed 5G) and data transfer is in the central role in the future distribution networks where IEC 61850 is very topical in Smart Grids standardization. Implementing IEC 61850 communication protocols (GOOSE, SV, MMS) and their possibilities for transmitting of different kind of data offers new opportunities for upgrading IEDs and distribution automation systems.

As a conclusion there are available very powerful tools for individual domains, but a mixture of different tools are required for simulating Smart Grids in all its aspects (e.g. power grids, markets, ICT, weather, regulation, societal systems), and composed in relevant use cases. There is a need for different comprehensive RT simulation platforms for integrating different types of models and connected into real environment.

Further, in order to make smart grid operation smarter, it will requires more advanced distributed active DMS than have been used in the past. These advanced distributed active DMS and preasigned communication system would allow maximal integration of DERs, making the most of existing grid while keeping the power security standards upon the associated advance monitoring and controlling functions. Distributed active DMS in general may include the monitoring and control functions as follows:

1. Monitoring, capabilities to monitor and gather the available information such as, state/mode, voltage, current, frequency, power factor and other operation parameters based on direct client-server or publisher-subscriber communication.
2. Data processing, which is one of the most important features that need to be fulfilled by distributed active DMS, since large amount of real-time data need to be handled.
3. Estimation, suitable state estimation tool need to be designed and inaccurate data compensation function need to be defined.
4. Controlling, capability of execution control algorithms in order to determine dispatch actions

that are needed for active components to fulfil real-time distribution managements' operation requirements.

The Figure 7 illustrates the active DMS IEDs with the available features in power distribution network based on the IEC 61850 standard that offered full interoperability among different vendor IEDs.

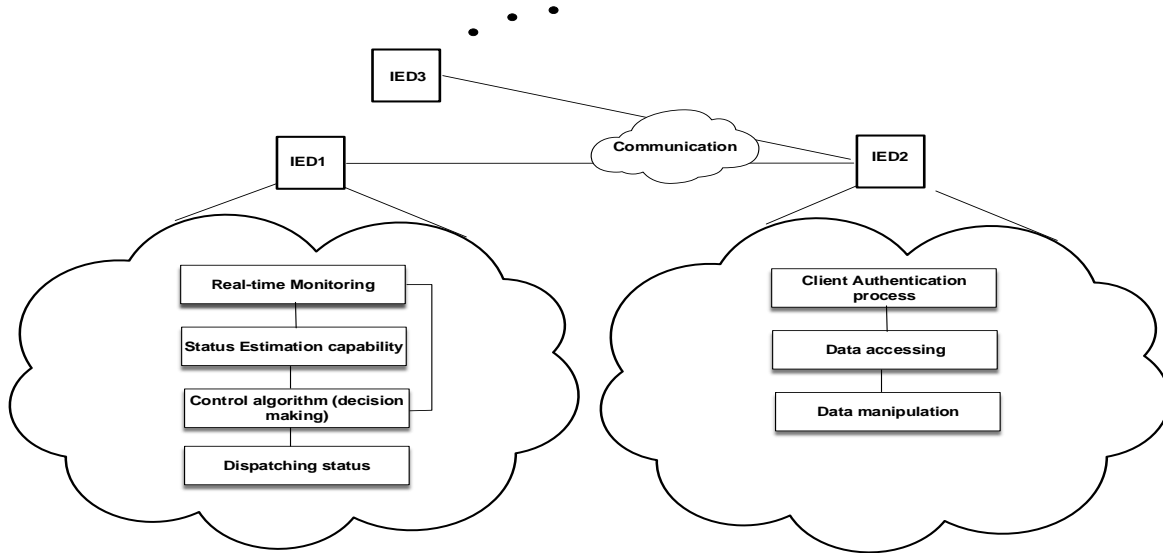


Figure 7. Distributed DMS IEDs overall concept.

4 Executed Tests and Experiments

The executed tests were both offline simulations and real-time simulations. The offline simulations were performed by Simscape Powersystems as well as by eMegasim + ePhasorsim. The real-time simulations were performed for SIL and CHIL testing by OP5600.

The test case study and the automation/control system are modelled using the Simscape PowerSystems (MATLAB/Simulink) Toolbox. SPS is a dedicated tool for modelling and simulating power systems and IEC 61850 communication blocks. Another motivation behind using SPS toolbox is because the models built in SPS are compatible with Opal-RT eMEGAsim real-time simulator and can be executed in opal RTlab software in real time.

Opal-RT has the provision to publish and subscribe to GOOSE messages. Active power P and reactive power Q was read from the predefined electrical connected point inside the model and capsule, published using the IEC 61850 GOOSE protocol. Two case studies had been defined one SIL and other is CHIL. In SIL case GOOSE subscriber blocked was configured and integrated inside the model to subscribe to GOOSE published from the model. The role of this GOOSE subscriber block was to subscribe to the GOOSE from the model and extract the P and Q measurements. These measurements were injected to the controller block inside the model based on the SIL.

Whereas, in CHIL case study the GOOSE subscriber was designed and built in different embedded instruments. These instruments are, the first one is a Beagle Bone Black (BBB) from the Texas National Instruments, and the second is the FPGA from Intel. The role of these embedded instruments was to subscribe to the GOOSE from the model and extract the P and Q measurements, execute the control function inside the device and publish the dispatching decision over another GOOSE messages as illustrated in the Figure 8 The round trip GOOSE latency was calculated for the overall completed tests.

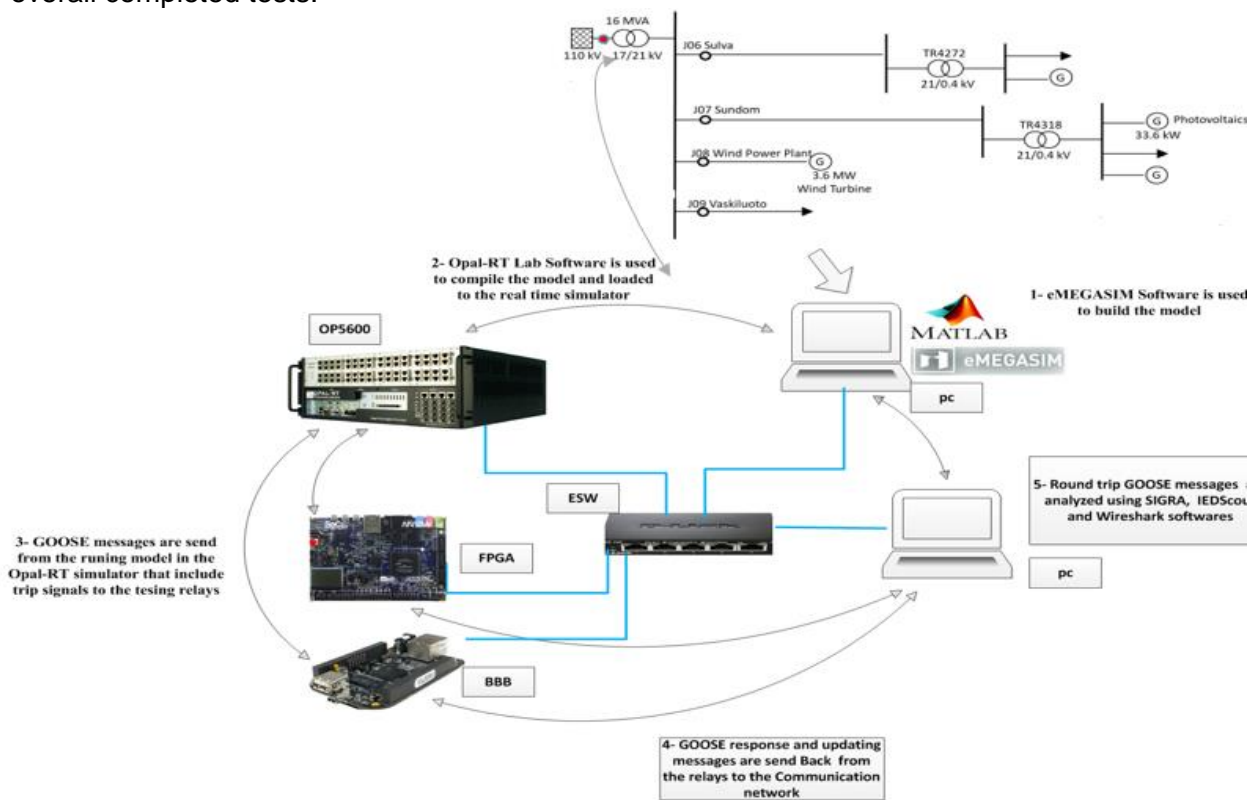


Figure 8. Distributed DMS IEDs setup platform and goose round trip concept.

4.1 Test Plan

For this project several types of scenarios, simulations and tests were developed. First different scenarios were developed by Simscape Powersystem as pre-work. The whole year power flow was simulated and the different type of control actions was implemented as open loop control method. Next, the similar models and scenarios were developed in eMegasim and ePhasorsim (the distribution network as well as the control system models). These developed models were simulated offline. The results from offline simulations were analysed for validating the developed models against the Simscape Powersystem models. All the different scenarios are presented in the Table 2.

Table 2. The simulation scenarios.

Scenario	Base network scenario	WT converter RPW control	WT converter RPW+NDZ control	1.75 MVar SR	PV inverters $\cos\phi$ control	PV inverters RPW+NDZ control
2018s1	X					
2018s2		X				
2028s1	X					
2028s2				X		
2028s3				X	X	
2028s4		X		X		
2028s5			X	X		
2028s6		X		X	X	
2028s7			X	X	X	
2028s8				X		X
2028s9		X		X		X
2028s10			X	X		X
2035s0	X					
2035s1				X		
2035s2				X	X	
2035s3			X	X		
2035s4			X	X	X	
2035s5				X		X
2035s6			X	X		X
2035s7						X
2035s8			X			X

Next, the aim of the real-time simulation tests was to test the developed controller and the platform as SIL and CHIL. SIL simulation test results were analysed against Simscape Powersystem results as well as offline simulation results. For CHIL tests, the communications between the controller and the simulated power system was IEC61850 Goose. The CHIL test plan was following:

1. RPW control for WT converter in Scenario 2018/2
 - a. Controller set-up parameters according to TSO limits
 - i. BeagleBoneBlack (BBB) controller
 1. $T_d = 1$ s read from file corresponding to 1 h input data
 2. $T_d = 0.1$ s
 - ii. FPGA controller

1. $T_d = 1$ s
2. $T_d = 0.1$ s
- b. Controller set-up parameters according to TSO limits ± 50 kVAr
 - i. BeagleBoneBlack (BBB) controller
 1. $T_d = 1$ s read from file corresponding to 1 h input data
 2. $T_d = 0.1$ s
 - ii. FPGA controller
 1. $T_d = 1$ s
 2. $T_d = 0.1$ s
2. RPW control for WT converter in Scenario 2028/4
 - a. Controller set-up parameters according to TSO limits
 - i. BeagleBoneBlack (BBB) controller
 1. $T_d = 1$ s read from file corresponding to 1 h input data
 2. $T_d = 0.1$ s
 - ii. FPGA controller
 1. $T_d = 1$ s
 2. $T_d = 0.1$ s
 - b. Controller set-up parameters according to TSO limits ± 50 kVAr
 - i. BeagleBoneBlack (BBB) controller
 1. $T_d = 1$ s read from file corresponding to 1 h input data
 2. $T_d = 0.1$ s
 - ii. FPGA controller
 1. $T_d = 1$ s
 2. $T_d = 0.1$ s

From the RT simulations the aim was to gather the results from P_{HVavg} , Q_{HVavg} , P_{HV} , Q_{HV} , P_{WT} , Q_{WT} and voltages 110 kV, 21 kV and 400 V. From the IEC 61850 GOOSE messages, the aim was to gather pcap files from the traffic between the controller and the RT target.

For the IEC61850 communications, the test procedure was following:

1. Update the RTlab software to version 11.3.3.63, and activate the RTlab software
2. Run the new RTlab version and test the IEC 61850 driver
3. Test the previous IEC 61850 based Matlab/Simulink solution
4. Design new .icd file for the GOOSE server
5. Generate new project file based on the new .icd
6. Run and test the GOOSE server that can subscribe – make control decision – publish GOOSE message
7. Integrate the communication system to the RTlab model for SIL and CHIL
8. Run the overall models and save the result
9. Change the control parameters (RPW limits) and generate new project based on the new control window
10. Run the model and save the result

4.2 Standards, Procedures, and Methodology

The standards implemented for communications was IEC61850 for Goose. Since published, IEC 61850 standard becomes one of the most promising and powerful solutions for the existing power industry limitations and expected to support energy systems evolutions. The key point it provides a uniform framework for all the related system levels. IEC61850 takes considerations for the all various aspects that are common at the substation site such as data models, communication solution, engineering and conformity over the channel. While organizing the data in terms of applications by means of syntax and semantics within the devices they did not specify it.

The main aspect that the IEC 61850 adopts with is the associated architectural construct “abstract-

ing” data object definition and its services. These data objects and their associated services have been abstracted independently from any underlying protocol that supports a comprehensive set of substation functions and provides strong services in order to facilitate the energy system communication. The abstract definitions of the data object allows mapping it to any protocol that can meet the best data and service requirements as IEC 61850 standards did not specify any protocol. Therefore, IEC 61850 specification can be capsule into three major focusing issues, firstly, standardizing the available information (data object model), substation functions (functional model) and IEDs name in which that provides to the IEDs a shared vocabulary that support the intended semantic meaning. Secondly, standardizing different ways of the accessing scheme to the available data abstract communication services interface (ACSI). These ways are defined as services that need to map over the assigned communication services and protocols. Lastly, defined a language eXtensible Markup Language (XML) implemented to describe all the configuration information exchanged between IEDs, network and power system.

While, the energy systems are moving into the digital environment where the huge amounts of real-time information data are available that allows a new kind of calculation for higher-level substation functions based protection and automation. IEC 61850 standard is unique, which designed from the base up to operate over the state-of-the-art technologies. It provides a novel set of functionalities, which are not, exists within the legacy SAS operation. From IEC 61850 implementation point view that attempts to utilize the fullest functionality, numerous of benefits will be achieved that included but not limited.

1. Open system for protection automation and data sharing by using the standard representation for the whole energy system objects and a common technology infrastructure to eliminate the procurement ambiguity.
2. Interoperability between devices from various manufacturers within the energy system and the ability to configure the system with the available configuration system tools independently from the on-site manufacturer support.
3. Secure and dependable overall system by means of several techniques that allows flexible information transfers
4. Reduce operation and maintenance overall system costs.
5. Flexible and expandable functions, easy adaptation by means of self-description in a standardized manner.

The IEC 61850 configuration process can seem like an impenetrable fog. The steps of the configuration process are intuitive and straightforward. Where, these configuration steps become gradually more complicated when the various details of the communication data objects are added to the designed IED (GOOSE server final project file). With these details the IEC 61850 standard tries to specify how the communicating IEDs, must work together and to get in the way that can read and write to/from data model tree. In addition, make the designed IEDs to implement various features as products in a competitive commercial environment. The main steps of the configuration process are the following.

1. List the required LNs and data modelling objects and generate the .icd file.
2. Describe how the designed IEDs or controlling instruments are integrated to the system and data flowing.
3. Configure monitoring control (and protection) functions in the designed IEDs.
4. Configure the designed IEDs to publish and subscribe data (in our case GOOSE protocol).
5. Configure the designed IEDs to extract data from the receiving GOOSE, and to use that data.
6. Generate the executed file from the configured .icd and main c file and collected in one project file.
7. Run the executed files for the project.

The order of these steps is flexible. Depending on the designed IED level and supporting functions

included in the configuration process, specific steps must be completed before specific other steps. The set of variables and signals in a given designed IED forms the data model of that IED when it is represented in a way specified by the IEC 61850 standard. Selected signals and variables from the data model of a given IED are grouped into data sets, and then communicated to other IEDs in data streams. Each data stream has one sending IED and possibly several receiving IEDs. IEC 61850 communication always uses one of the standard's protocol mappings, so that the used specifies which communication protocol, such as GOOSE, is used in our case study to deliver the messages. IEC 61850 standardizes how data is represented in communication, how communication is configured, and how the data is transferred. The designed IEDs will almost certainly need other configuration parameters as well. These parameters are configured using the predefined XML and C languages based on the configuration process.

The configuration of IEC 61850 communication between IEDs consists of several steps, which are partly independent of each other. Some steps need to be done before certain other steps, but in general, the steps can be done in any order. The order in which the steps are performed can be described as following the "top-down approach," the "bottom-up approach," or the "mixed approach." In the top-down approach, the configuration process begins with the general features of the automation system and proceeds towards the details. In fact, the top-down approach begins when the automation system is still being designed. The bottom-up approach does the opposite by starting with the details, and by having them gradually form a larger whole. In the mixed approach, the configuration process follows neither of these two. The user does not have to stick to the selected approach. Instead, researcher can "mix" the different approaches freely. In our case study "bottom-up approach is used.

libiec61850 open source library is used to configure the GOOSE server. This open source library is like roles: a given piece of software may handle more than one role, and thus, in a sense, contain more than one monitoring control functions in a project file. SCL is an XML-based language, specified in the standard, for storing configuration information in computer files. This language is used in five different file types, each intended to contain different pieces of the substation's configuration. There are two versions of this language, and these versions are not compatible. Each project must select which version is used in the SCL files, and use the same version for all files.

The project start with system design phase, during which a project design engineer plans how the automation system will fulfill the requirements set for it. He or she will choose the system architecture, what physical devices or IEDs will be used in the system, and how those instruments will communicate with each other. When the design engineer chooses which IED types are used in the automation system, researcher needs to know the capabilities of the IEDs. The capabilities of a given candidate IED are described by an ICD file, which uses the SCL language. The design engineer validate the ICD files and build the project files. Next step is to select such a combination of IEDs that together they cover all the required functionality. While, upon the setup platform, the user should decide which IEDs perform which pieces of functionality in the automation system by map-ping the logical nodes to the IEDs which perform the associated function. Lastly, One of the main tasks of the designed automation system operator is to set up the IEC 61850 communication between the IEDs based on the selected IEC 61850 protocols (GOOSE, SV and MMS). In order to send the value of a given signal or variable in IEC 61850 communication, the signal must be included in the sending IED's data model. Adding a signal to the IED's data model require the use of the .icd file modification. Once the automation system configuration is done, now need to set how the designed IEDs use the signals they receive using IEC 61850 communication.

Procedures and used methodologies for the simulations are explained in Chapters 2.1, 2.2, 4.3 and 5.

4.3 Test Set-up

The RT co-simulation platform for TA laboratory is presented in Figure 9. The platform consists of RT power system simulator to model grid, corresponding controllers and communication protocols. The simulation platform had the capability to model the grid (in phasor domain) and controllers (in time domain). The system was OPAL OP5600 HW with eMegasim (time domain) and ePhasorsim (phasor domain) environments via Simulink/Matlab and RT-Lab software.

The host infrastructure provided the 61850-GOOSE interface in the RT simulator to enable the simulated model to communicate to real control hardware. The programmed HW controller on Beaglebone to the simulation environment. A local area network (LAN) setup for the communication network was established. This communication network included the controller implemented on Beaglebone HIL controller and OP5600 simulator.

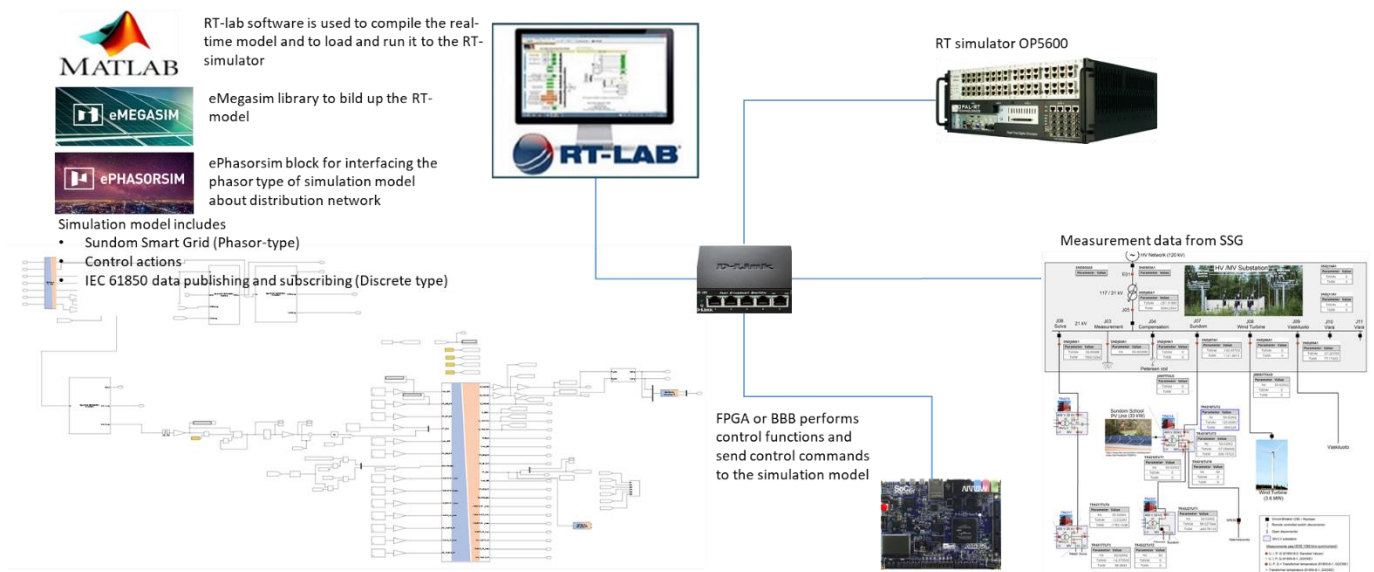


Figure 9. Outline of the developed real-time co-simulation environment.

4.4 Data Management and Processing

The developed real-time simulation models were for SSG 2018 and 2028 scenarios. The RPW controller was implemented as SIL as well as CHIL for Scenario 2018/2 and Scenario 2028/4. The simulation models and results are maintained by UVA. The aim is to publish a scientific paper based on these results. A demo model, Scenario 2018/2 is given the use of Offis.

5 Results and Conclusions

The results presented are simulation results of Simscape Powersystem, eMegasim + ePhasorsim offline, SIL real-time and CHIL real-time.

5.1 Developed use cases by Simscape Power Systems

At the first phase, different use cases were developed for investigating the operation of power system as well as the RPW and NDZ controllers. These use cases were modelled by Simscape Powersystem in order to have the understanding about behaviour of the system(s), for evaluating the interesting use cases for the real-time simulations as well as for generating the initial values for the Powerfactory models (for ePhasorsim block). The controls in these simulation were done as open loop, because closed loop simulations did increase the simulation time greatly.

5.1.1 Scenario 2018/1 – Situation 2018

Situation 2018 was the base case or the state of the art. This case is called Scenario 2018/1 later in this report. The aim of this use case was to validate the simulation results to be consistent with the real measurements from SSG. Hourly average values of measured active power 1.5.-2018 – 31.4.2018 was used as load data in the model. The load profiles of feeders J06 Sulva, J07 Sundom and J09 Vaskiluoto are presented in Figure 10, Figure 11 and Figure 12 respectively.

In the same way hourly average values of measured active power generation of wind turbine (WT) was used in the model as the generation data. The WT generation profile is presented in Figure 13. Active power generation of photovoltaic (PV) system at Sundom school (33.6 kWp) was modelled based on solar irradiation data. The PV generation profile is presented in Figure 14.

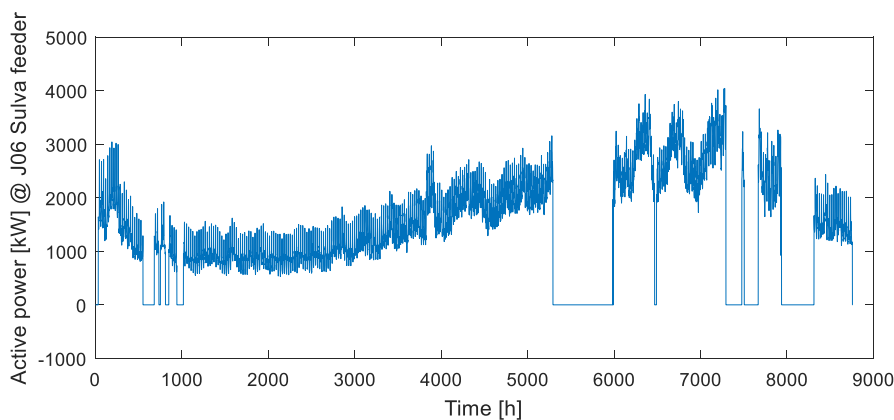


Figure 10. Measured load at J06 Sulva feeder.

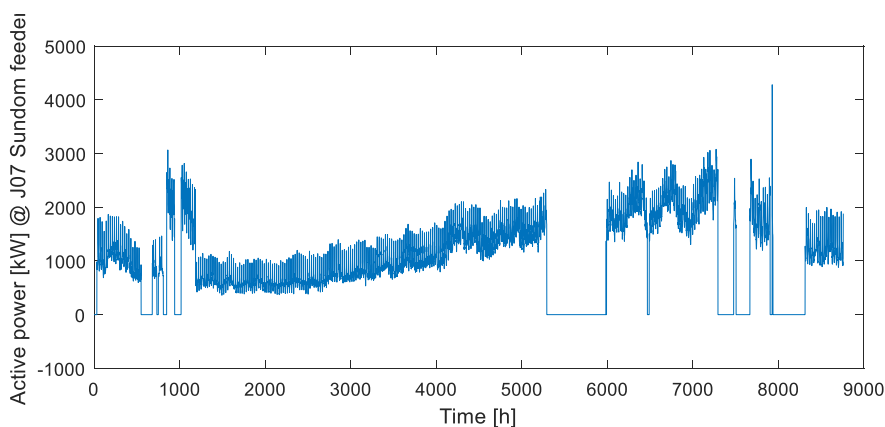


Figure 11. Measured load at J07 Sundom feeder.

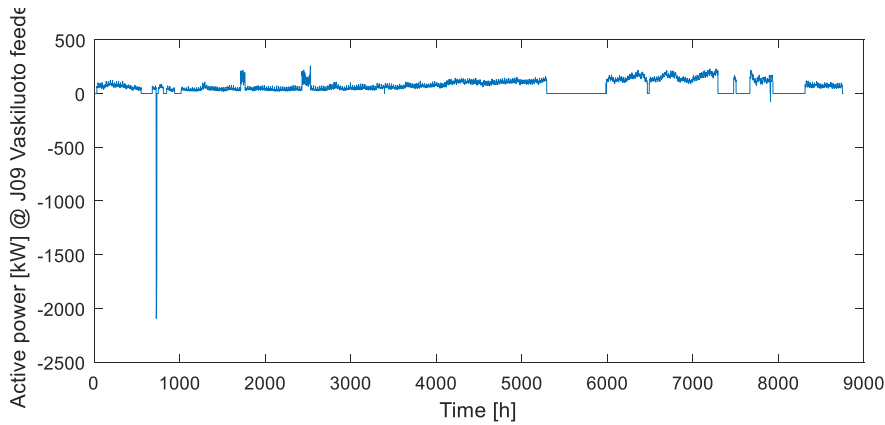


Figure 12. Measured load at J09 Vaskiluoto feeder.

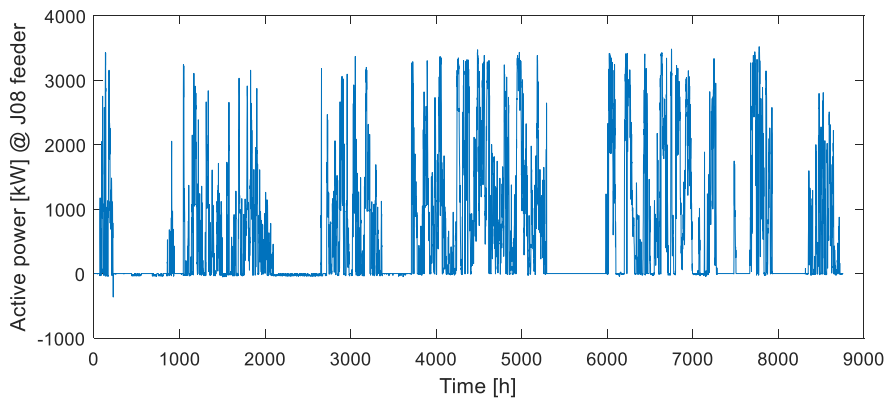


Figure 13. Measured wind power generation.

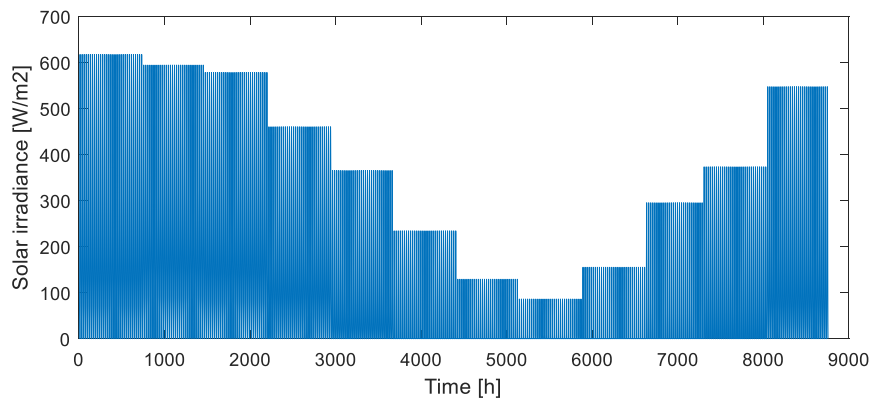


Figure 14. Simulated PV generation for Sundom school PV unit.

Based on the simulation, the simulated active power flows were consistent with measured data as can be noticed in Figure 15. In the simulation model, the load type was selected to be constant power factor type. Therefore, the power factors for loads were estimated by simulating one-year power flows with different values of power factors. The values of power factors were 0.998, 0.995, 0.990, 0.895 and last average values based on one-year measurements from the feeders J06, J07 and J09. The best results gave $\cos\phi = 0.995$ for all loads, which is presented in Figure 16. Voltages are presented in Figure 17 and Figure 18.

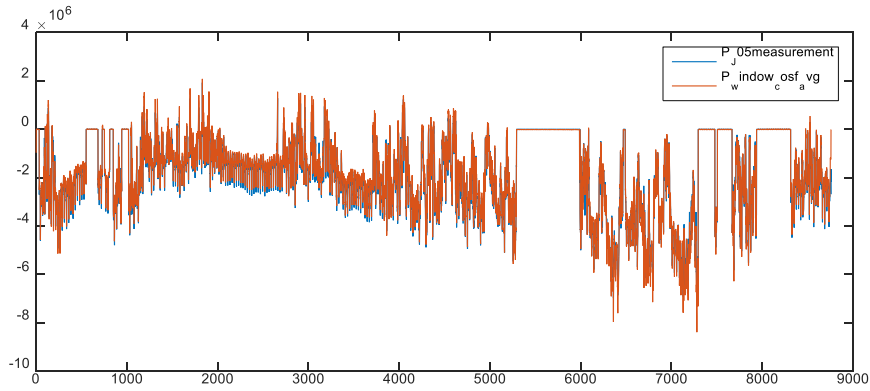


Figure 15. Simulated and measured active power flows at 21 kV bus in Sundom Smart Grid.

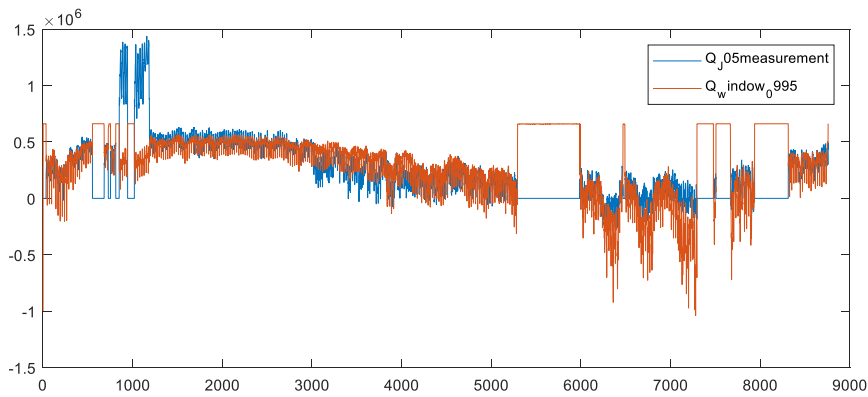


Figure 16. Simulated and measured reactive power flows at 21 kV bus in Sundom Smart Grid. Power factor of loads was set up 0.995_{ind} .

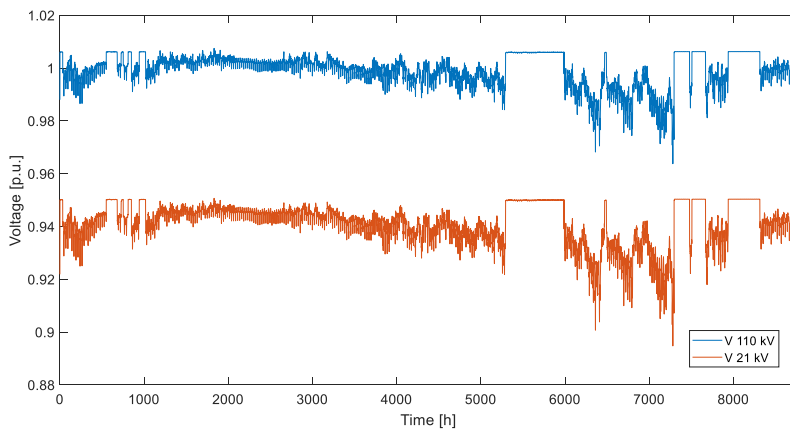


Figure 17. Voltage in 110 kV and 21 kV bus in Scenario 2018/1.

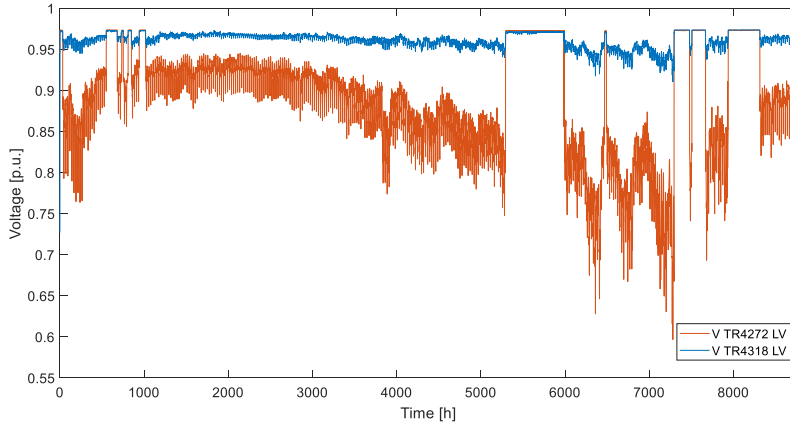


Figure 18. Voltage in 0.4 kV bus in Scenario 2018/1.

In Figure 19 is presented the reactive power window at 110 kV connection point from a) the measurement data and b) the simulation results. In Figure 20 is presented the reactive power window at 21 kV bus bar respectively. It can be noticed, that the results are quite similar, only the constant load type did affect the results, in reality the loads are voltage dependent and determination of the parameters p and q in:

$$P_i^* = P_i(v_i)^p \text{ and } Q_i^* = Q_i(v_i)^q.$$

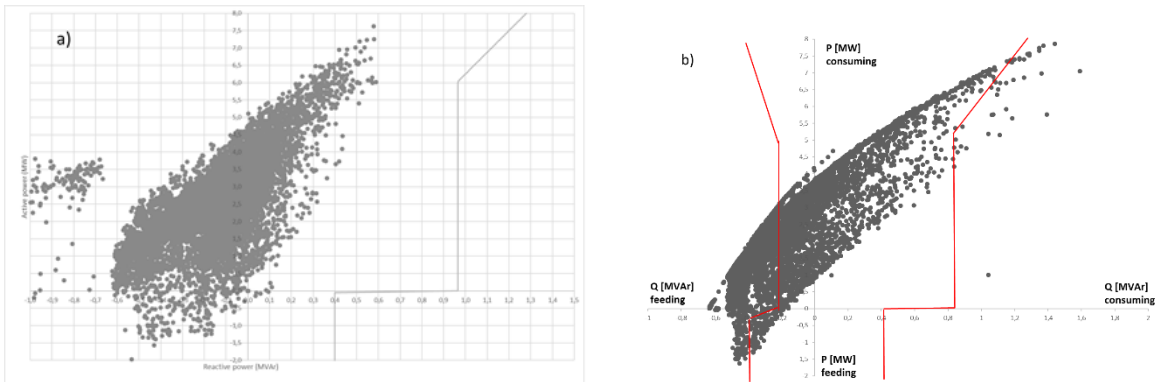


Figure 19. Reactive power window at 110 kV connection point of SSG from a) the measurement data and b) the simulation results.

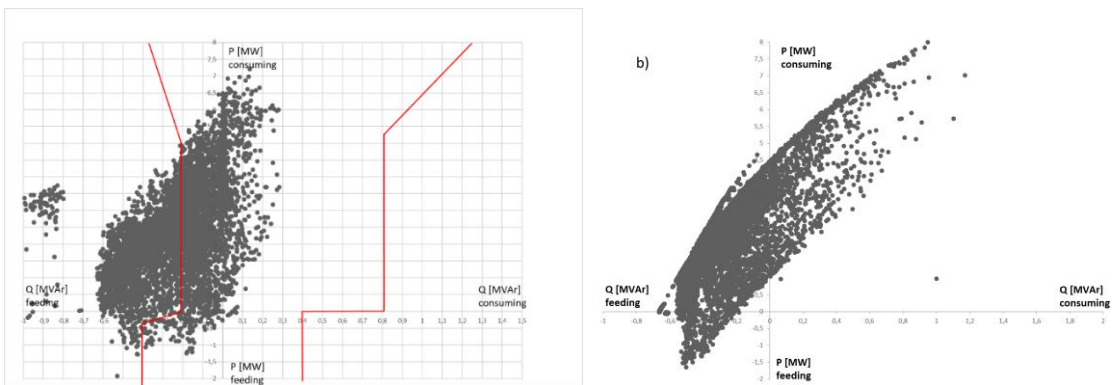


Figure 20. Reactive power window at 21 kV bus of SSG from a) the measurement data and b) the simulation results.

5.1.2 Scenario 2018/2 – RPW control

In this scenario RPW control was implemented through the WT converter. In Figure 21 is presented the result of the simulation when the magnitude of the reactive power for WT converter Q_{set} was set to be opposite from the measured Q_{HV} value if the reactive power according to active power (Q, P) point was out of the window. In the Figure 21 it can be noticed that all the points out of the window were controlled to “zero”.

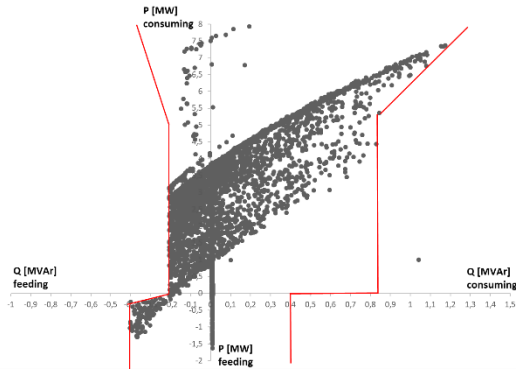


Figure 21. Reactive power window at 110 kV side in Scenario 2018/2.

5.1.3 Scenario 2028/1

In scenarios 2028 the grid model developed by increased cabling, loads as well as PV generation up to 2.6 MWp in total at feeders J06, J07 and J09 comprising of about 740 units and share of customers 25 %. Line lengths and types according to the plan of increasing cabling degree is presented in the Table 3, peak load forecasts is presented in Table 4, and PV generation forecasts is presented in the Table 5.

Table 3. Line lengths of Sundom Smart Grid.

Feeder	Overhead [m]	Cable [m]	Sum [m]	Cabling degree
J06 Sulva	25246	7938	33184	23,9 %
J06 Sulva 2028	0	40756	40756	100,0 %
J07 Sundom	12950	10199	23149	44,1 %
J07 Sundom 2028	8200	16372	24572	66,6 %
J08 Wind	0	733	733	100,0 %
J09 Vaskiluoto	5913	1122	7035	15,9 %
J09 Vaskiluoto 2028	3340	4467	7807	57,2 %
Total 2018	44109	19992	64101	31,2 %
Total 2028	11540	62328	73868	84,4 %

Table 4. Forecasts for peak loads of Sundom Smart Grid.

	Pmax [MW]			Factors regarding to 2018 situation	
	2018	2028	2035	2028	2035
J06 Sulva	5,108	6,2104	6,517	1,215818324	1,2758418
J07 Sundom	3,876	3,876	4,296	1	1,1083591
J09 Vaskiluoto	1,214	1,214	2,054	1	1,6919275

Table 5. Forecasts for PV units increase of Sundom Smart Grid.

	2020 / 10%			2030 / 25%			2035 / 50%		
	Units	P [kWp]	A [m2]	Units	P [kWp]	A [m2]	Units	P [kWp]	A [m2]
J06 Sulva	171	615	5491	357	1285	11471	357	2569	22942
J07 Sundom	113	406	3623	258	927	8281	258	1855	16562
J09 Vaskiluoto	11	39	352	122	438	3913	122	876	7825
Total	294	1060	9466	736	2650	23664	736	5301	47329

The simulation results, the reactive power window at 110 kV side and at 21 kV side as well as voltage profiles are presented in Figure 22 - Figure 24. It can be noticed that the increased cabling increase capacitive reactive power in the HV/MV connection point and almost all the (Q, P) points are out of the window. Also the effect for voltage level at the secondary transformers.

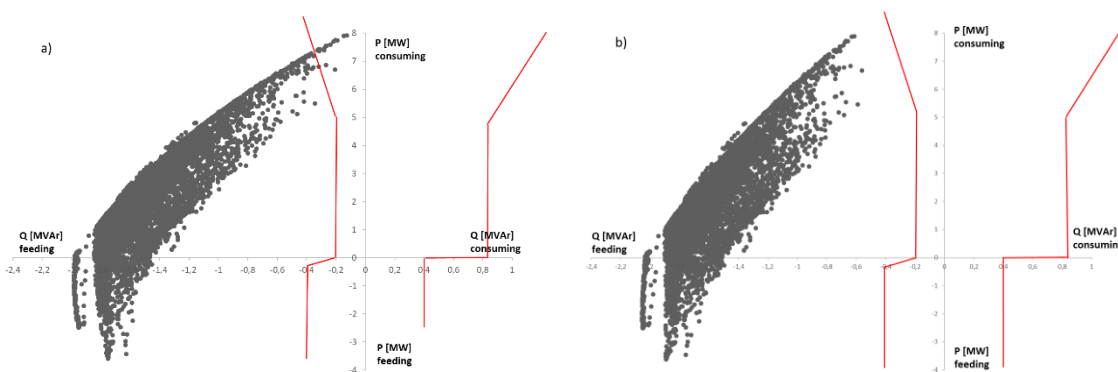


Figure 22. Reactive power window at a) 110 kV b) 21 kV side for SSG in Scenario 2028/1.

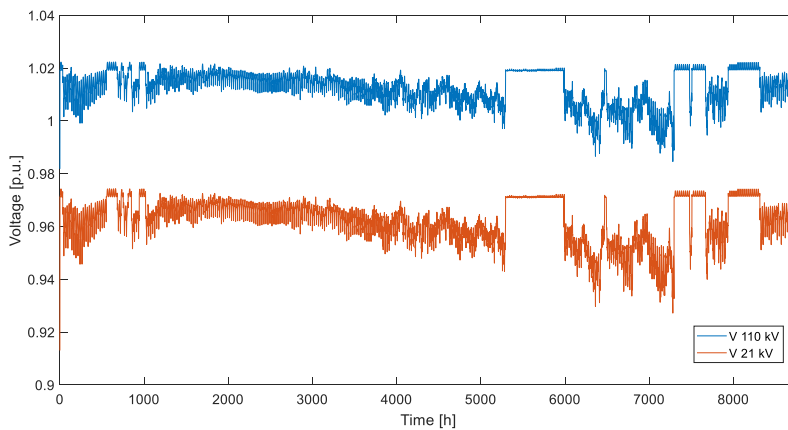


Figure 23. Voltages at 110 kV and 21 kV bus in Scenario 2028/2.

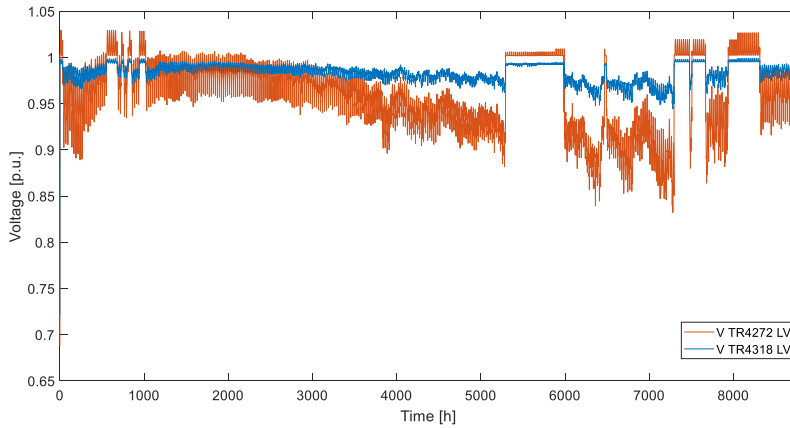


Figure 24. Voltage at secondary transformers TR4272 and TR4318 400 V bus.

5.1.4 Scenario 2028/2 – SR

For compensating the reactive power injection, a shunt reactor (SR) was dimensioned to the network when there was no reactive power consumption than loads. The power factor for the loads was 0.995. In Figure 25 is presented the reactive power window from the simulation results when a) SR was 1.5 MVar and b) 1.75 MVar. Based on these results, the 1.75 MVar SR was used for further studies.

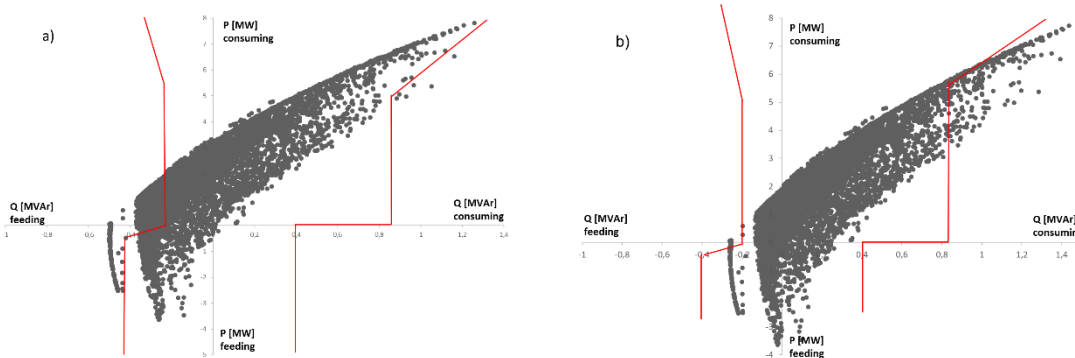


Figure 25. Reactive power window for SSG with a) 1.5 MVar and b) 1.75 MVar shunt reactor in Scenario 2028/2.

5.1.5 Scenario 2028/3 – SR and $\cos \phi$ control of PV inverters

This case was like previous case but now the reactive power of the PV inverters were controlled by the constant power factor 0.95_{ind} . The results of the simulation is presented in Figure 26.

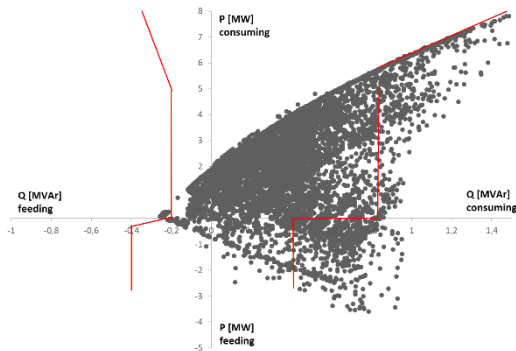


Figure 26. Reactive power window in Scenario 2028/3.

5.1.6 Scenario 2028/4 – SR and RPW control of WT converter

This case is like Scenario 2028/2, but in addition WT converter was controlled by the developed RPW controller. The simulation result is presented in Figure 27.

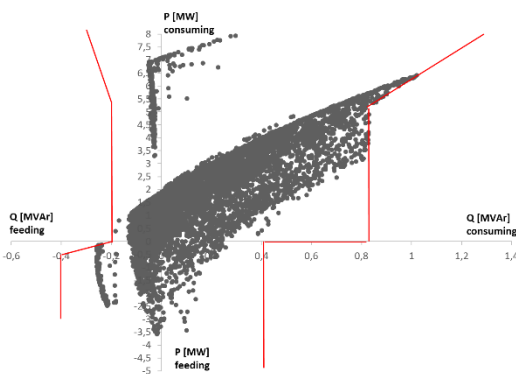


Figure 27. Reactive power window in Scenario 2028/4.

5.1.7 Scenario 2028/5 – SR and RPW+NDZ control of WT converter

This case is like Scenario 2028/2, in addition WT converter was controlled by the RPW as well as by the NDZ controller. The simulation result is presented in Figure 28.

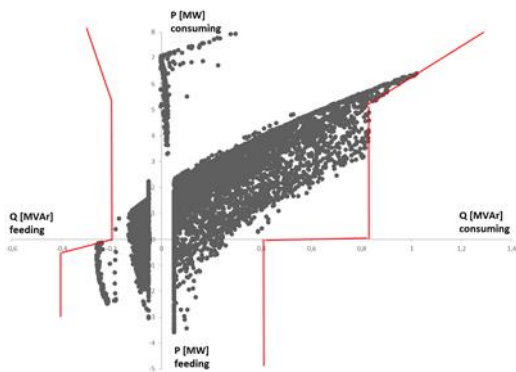


Figure 28. Reactive power window in Scenario 2028/5.

5.1.8 Scenario 2028/6 – SR, RPW control of WT converter and $\cos\phi$ control of PV inverters

This case is like Scenario 2028/2, in addition WT converter was controlled by the RPW and the PV inverters were controlled by the constant power factor 0.95_{ind} . The simulation result is presented in Figure 29.

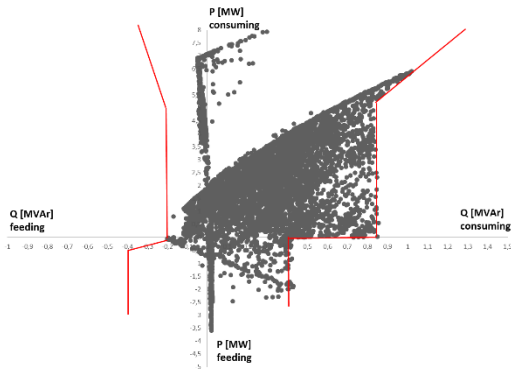


Figure 29. Reactive power window in Scenario 2028/6.

5.1.9 Scenario 2028/7 – SR, RPW+NDZ control of WT converter and $\cos\phi$ control of PV inverters

This case is like Scenario 2028/2, in addition WT converter was controlled by the RPW and by the NDZ controller as well as the PV inverters were controlled by the constant power factor 0.95_{ind} . The simulation result is presented in Figure 30.

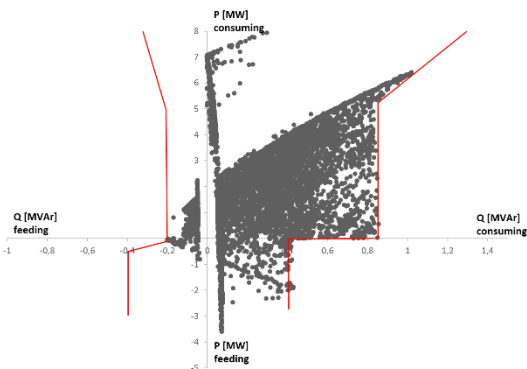


Figure 30. Reactive power window in Scenario 2028/7.

5.1.10 Scenario 2028/8 – SR and RPW+NDZ control of PV inverters

This case is like Scenario 2028/2, but in addition, PV inverters were controlled by the RPW as well as by the NDZ controller. The meaning of this case study was to represent the situation where an MV feeder could form a microgrid. The reactive power windows at MV feeders J06 Sulva and J07 Sundom are presented in Figure 31. The active and reactive power flows at feeders J06 and J07 are presented in Figure 32 and in Figure 33 respectively, and from these figures it can be noticed that by setting maximum $\cos\phi = 0.95$ is inadequate and therefore the RPW+NDZ controls at MV feeders did not work perfectly. Next it would be interesting to make a study where $\cos\phi_{max} = 0.90$ or even $\cos\phi_{max} = 0.85$. The RWP at 110 kV side is presented in Figure 34, and it can be noticed of the effect of the PV inverters as well as SR of consuming the reactive power. It seems that by utilizing RPW+NDZ control for PV inverters, less is required for SR.

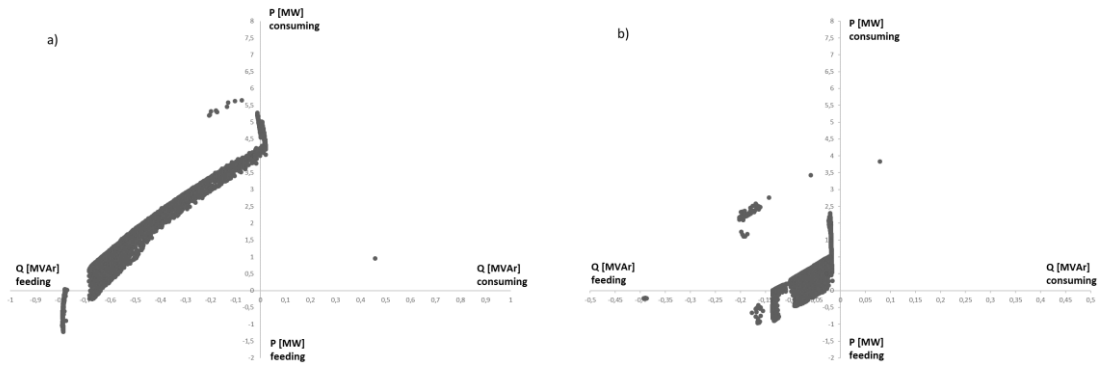


Figure 31. Reactive power window at a) J06 Sulva and b) J07 Sundom feeder in Scenario 2028/8.

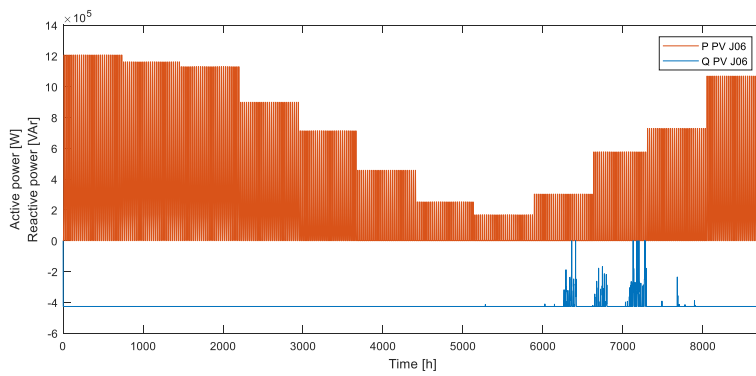


Figure 32. Active and reactive power at J06 Sulva feeder in Scenario 2028/8.

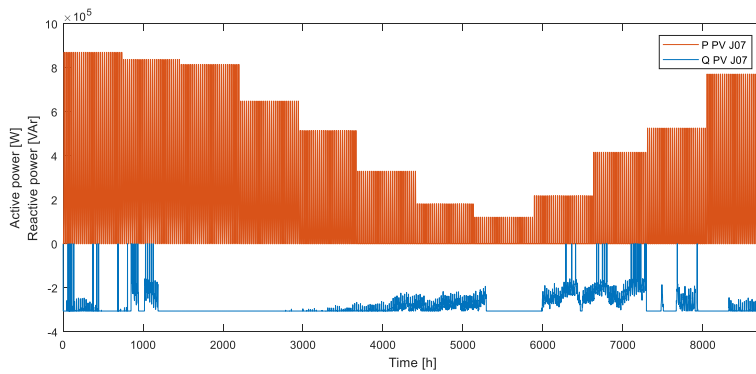


Figure 33. Active and reactive power at J07 Sundom feeder in Scenario 2028/8.

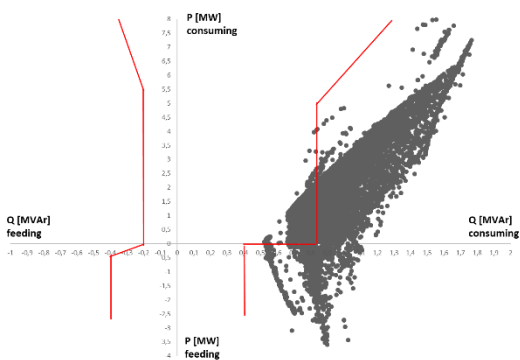


Figure 34. Reactive power window in Scenario 2028/8.

5.1.11 Scenario 2028/9 – SR, RPW control of WT converter and RPW+NDZ control of PV inverters

This case is like previous Scenario 2028/8, but in addition WT converter was controlled by the RPW controller. This use case illustrates the situation where an MV feeder could form a microgrid and in the same time, the reactive power is controlled in HV connection point for staying in the RPW. The simulation result is presented in Figure 35.

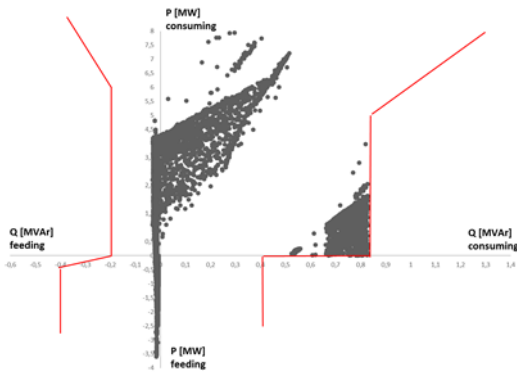


Figure 35. Reactive power window in Scenario 2028/9.

5.1.12 Scenario 2028/10 – SR, RPW+NDZ control of WT converter and RPW+NDZ control of PV inverters

This case is like Scenario 2028/8, but in addition WT converter was controlled by the RPW+NDZ controller. This use case illustrates the situation where an MV feeder could form a microgrid, or the whole MV grid could form a microgrid and in the same time, the reactive power is controlled in HV connection point for staying in the RPW. The simulation result is presented in Figure 36.

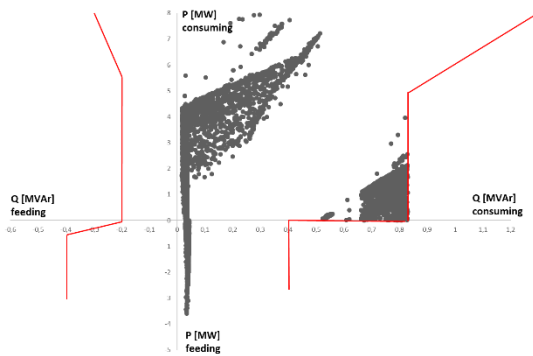


Figure 36. Reactive power window in Scenario 2028/10.

5.1.13 Scenario 2035/0

SSG model was developed further based on Scenario 2028/1 by increasing loads as well as PV generation up to 5.3 MWp in total at feeders J06, J07 and J09 comprising of about 1480 units and share of customers 50 %. The simulation result is presented in Figure 37.

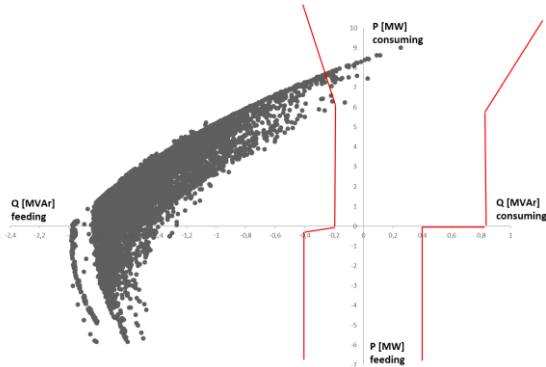


Figure 37. Reactive power window in Scenario 2035/0.

5.1.14 Scenario 2035/1 – SR

This scenario is based on the Scenario 2035/0, but in addition a 1.75 MVar SR was connected to the MV bus. The simulation result is presented in Figure 38.

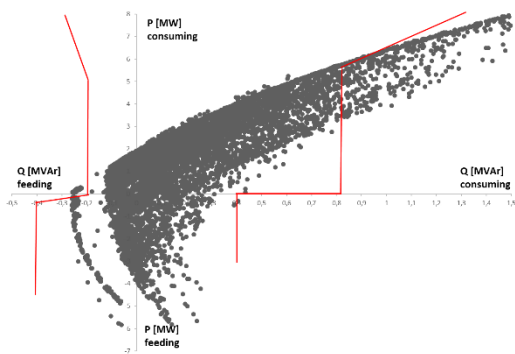


Figure 38. Reactive power window in Scenario 2035/1.

5.1.15 Scenario 2035/2 – SR and $\cos \phi$ control of PV inverters

This scenario is based on the Scenario 2035/1, but in addition the PV inverters were controlled by the constant power factor 0.95_{ind} . The simulation result is presented in Figure 39.

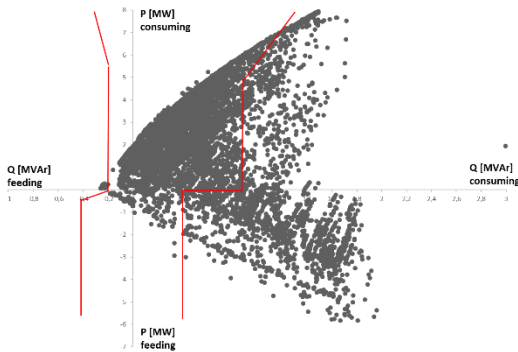


Figure 39. Reactive power window in Scenario 2035/2.

5.1.16 Scenario 2035/3 – SR and RPW+NDZ control of WT converter

This case is based on the Scenario 2035/1, but in addition, WT converter was controlled by the RPW as well as by the NDZ controller. The simulation result is presented in Figure 40.

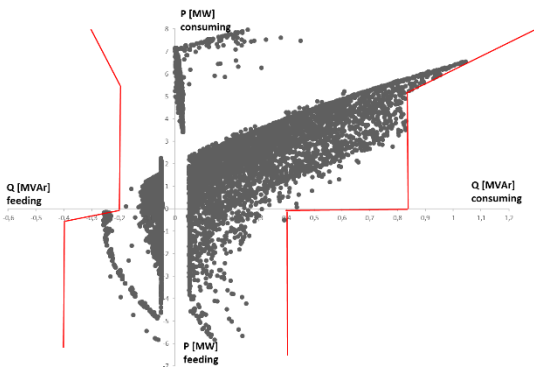


Figure 40. Reactive power window in Scenario 2035/3.

5.1.17 Scenario 2035/4 – SR, RPW+NDZ control of WT converter and $\cos \phi$ control of PV inverters

This case is like Scenario 2035/1, in addition WT converter was controlled by the RPW and by the NDZ controller as well as the PV inverters were controlled by the constant power factor 0.95_{ind} . The simulation result is presented in Figure 41 and in Figure 42, and they show that the WT converter cannot produce requested reactive power in every moment what PV inverters consume. It can be concluded it is not feasible to control PV units by constant $\cos \phi = 0.95_{ind}$.

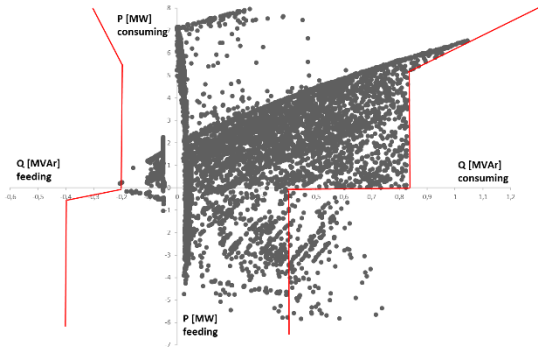


Figure 41. Reactive power window in Scenario 2035/4.

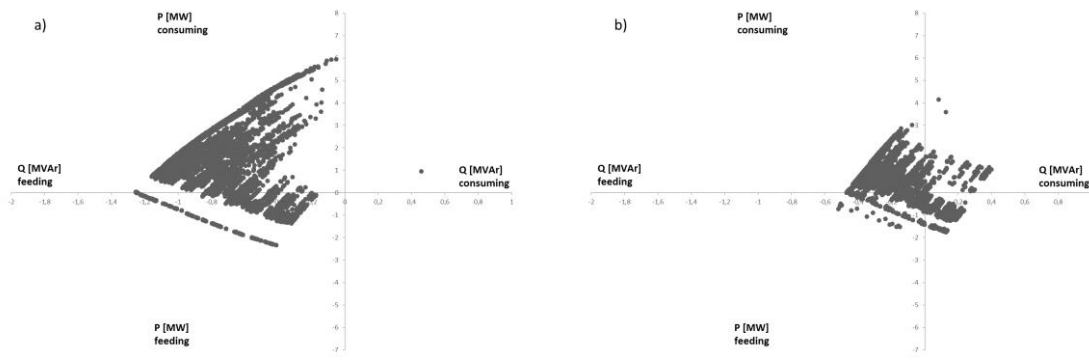


Figure 42. Reactive power window at a) J06 Sulva and b) J07 Sundom feeder in Scenario 2035/4.

5.1.18 Scenario 2035/5 – SR and RPW+NDZ control of PV inverters

This case is like Scenario 2035/1, but in addition, PV inverters were controlled by the RPW as well as by the NDZ controller. The simulation results is presented in Figure 43.

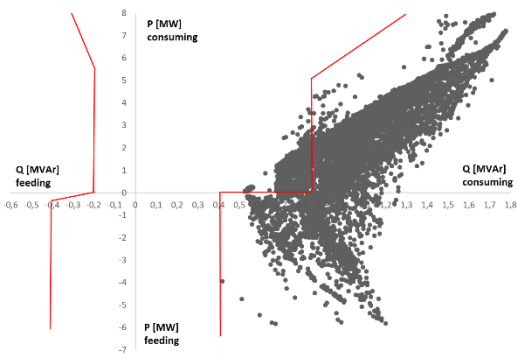


Figure 43. Reactive power window in Scenario 2035/5.

5.1.19 Scenario 2035/6 – SR, RPW+NDZ control of WT converter and RPW+NDZ control of PV inverters

This case is like Scenario 2035/1, but in addition, WT converter was controlled by the RPW+NDZ as well as PV inverters were controlled by the RPW as well as by the NDZ controller. The simulation result is presented in Figure 44.

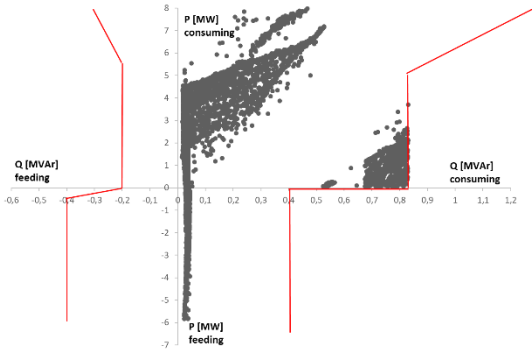


Figure 44. Reactive power window in Scenario 2035/5.

5.1.20 Scenario 2035/7 – RPW+NDZ control of PV inverters

This case is like Scenario 2035/0, but in addition, PV inverters were controlled by the RPW as well as by the NDZ controller.

5.1.21 Scenario 2035/8 – RPW+NDZ control of WT converter and RPW+NDZ control of PV inverters

This case is like Scenario 2035/0, but in addition, WT converter was controlled by the RPW+NDZ as well as PV inverters were controlled by the RPW as well as by the NDZ controller.

5.2 Offline simulations by RT-lab

The offline simulations of the real-time models was performed for validating the real-time models against the Simscapre Powersystem simulation results. The real-time models developed and the offline results are presented in the following paragraphs. The time step for data input was set up $T_s = 0.1$ s or $T_s = 1$ s and the type of the input data was either step function or interpolated. In the reactive power windows it is presented the hourly average values of reactive power and active power ($Q_{avg,h}$, $P_{avg,h}$).

5.2.1 Scenario 2018/1

This scenario was simulated when $T_s = 0.1$ s. The Figure 45 a) presents the same situation and similar set-up than in Figure 19 b). It can be noticed that the simulation results are almost equal. The slight difference between these results is because of that the measurement data as the input data was not available every moment. In Simscapre Powersystems simulations the missing data was replaced by zero values whereas in ePhasorsim simulations the missing data was replaced by the previous values. In addition, in the ePhasor block the primary transformer voltage was kept constant (based on slack bus value in the load flow calculations in Powerfactory) whereas in Simscapre Powersystems model the supporting network was modelled as the voltage source. This phenomenon can be noticed in Figure 48. In Figure 46 is presented the simulation results when the input data was interpolated.

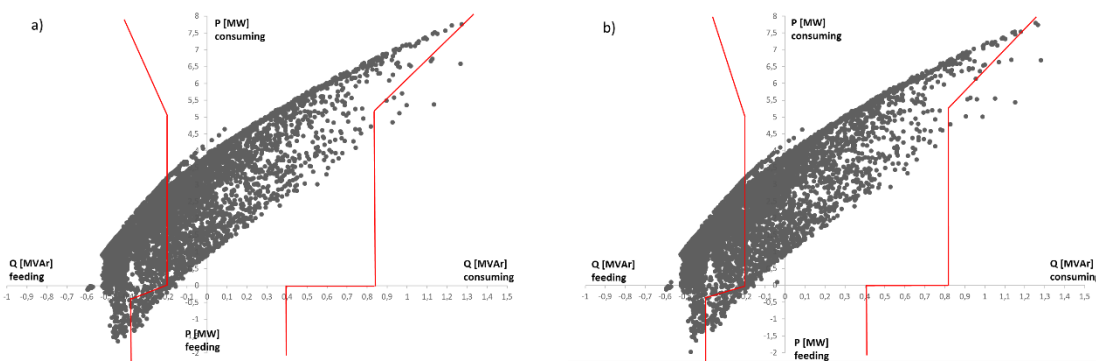


Figure 45. Reactive power windows in Scenario 2018/1 offline when $T_s = 0.1$ s when a) (Q_h , P_h) and b) ($Q_{avg,h}$, $P_{avg,h}$) and the input data was step function.

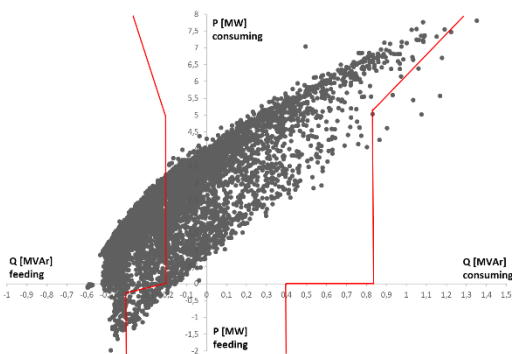


Figure 46. Reactive power windows in Scenario 2018/1 offline when $T_s = 0.1$ s when the input data was interpolated.

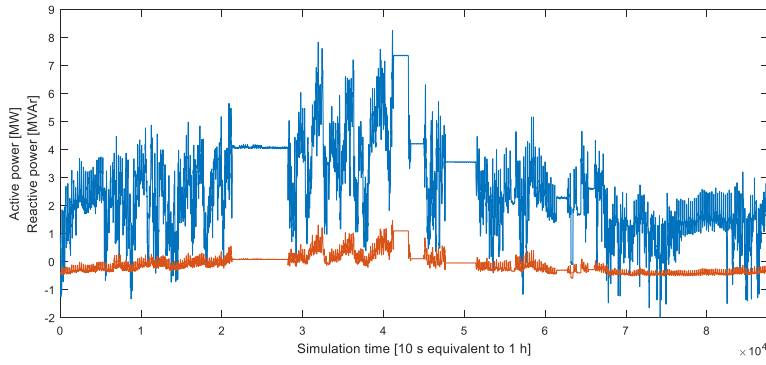


Figure 47. Active and reactive power flows at HV/MV connection point in Scenario 2018/1 offline, the input data was step function.

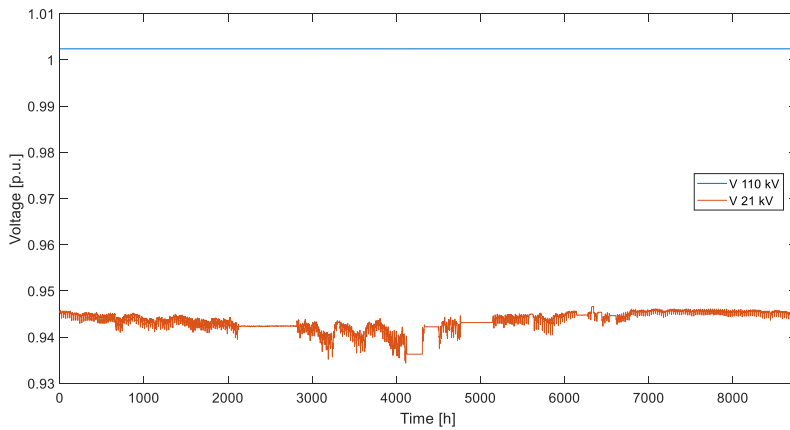


Figure 48. Voltage profiles at HV and at MV bus in Scenario 2018/1 offline.

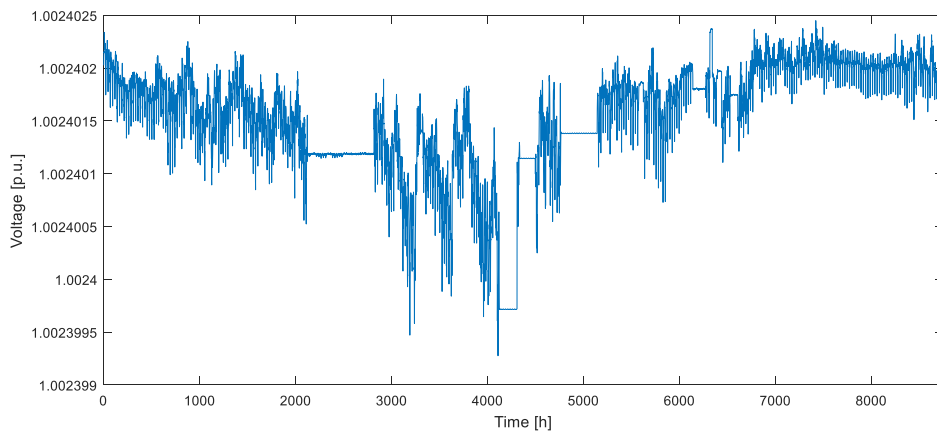


Figure 49. Voltage profiles at HV connection point in Scenario 2018/1 offline.

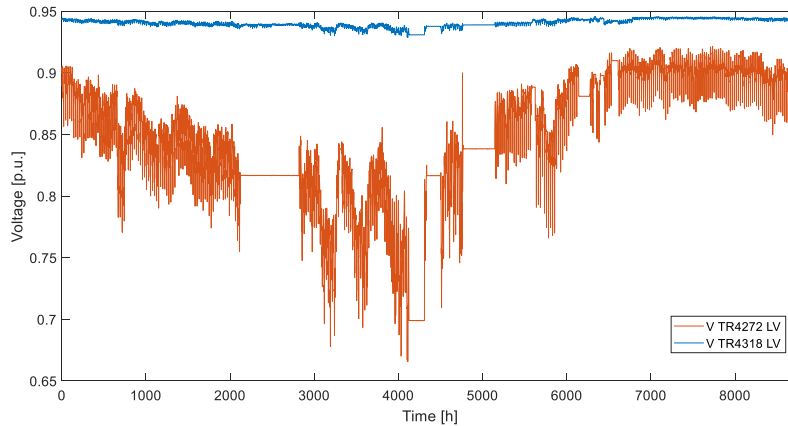


Figure 50. Voltage profiles at MV connection points in Scenario 2018/1 offline.

5.2.2 Scenario 2018/2

The offline simulations were performed as a closed-loop simulation for the SSG where the reactive power was controlled by the RPW controller. The controller include the algorithm almost as in Simscape Powersystems model. Now the measurement of reactive power of WT was connected for the closed loop simulations, in addition an I-controller was tuned for achieving stable system and a hold/memory block to maintain the current set value for Q_{WTset} as long as (Q, P) stayed inside the RPW.

The algorithm was tuned differing from the open loop model. Instead of driving Q_{WTset} to zero if the point were out of the window (as in Simscape Powersystem model) the algorithm gave Q_{WTset} to the RPW limits ± 50 kVAr. First, if the algorithm gave $Q_{WTset} = \pm Q_{HV}$ i.e. always tried to set reactive power to zero if the point was out of the window. This caused the reactive power of the WT to swing as well as at the 110 kV connection point. Therefore, the algorithm for Q_{WTset} was tuned so that the aim of the controller was to drive reactive power to the limits if (Q, P) was out of the window. Now the control was more peaceful.

Next, it was noticed that driving reactive power to the limits gave the results that all the points were not inside the window. This was due to the points were calculated as hourly average values and calculation was based on the simulation step from the 110 kV measurement point. Therefore, for these limits were added ± 50 kVAr. Now the controlled reactive power of the WT was even more peaceful.

In Figure 51 and in Figure 52 is presented the reactive power windows from the simulation results with the tuned controller. It can be noticed the difference of results against the open loop simulations (Figure 21). In Figure 53 is presented active and reactive power flows at HV/MV connection point. In Figure 54 and in Figure 55 is presented active and reactive power flows from the WT when input data was step type or interpolated.

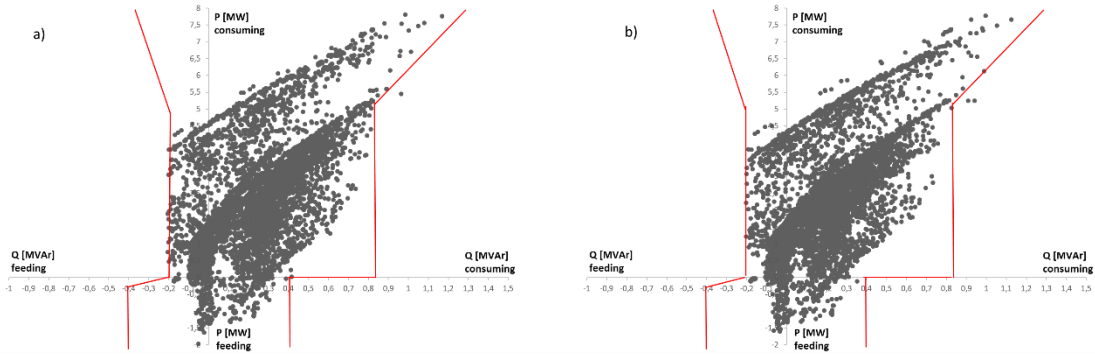


Figure 51. Reactive power window in Scenario 2018/2 offline when $T_s = 0.1$ s and a) input data was step function b) input data was interpolated.

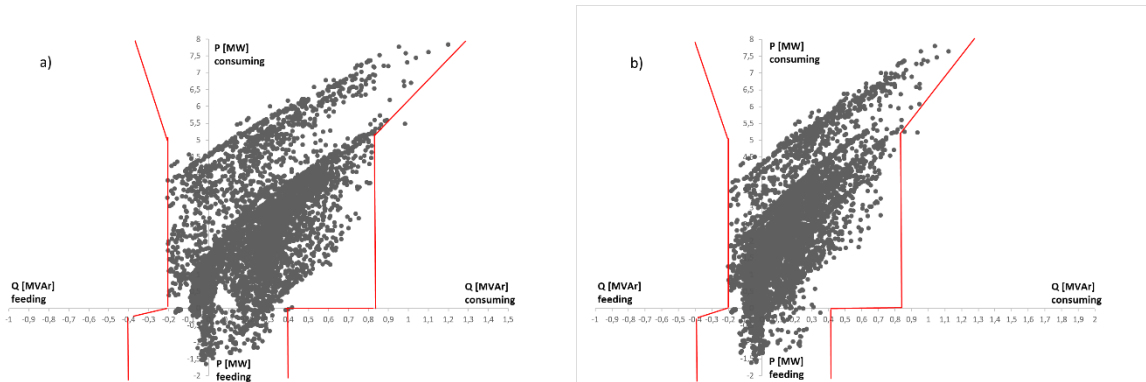


Figure 52. Reactive power window in Scenario 2018/2 offline when $T_s = 1$ s a) input data step function b) input data interpolated.

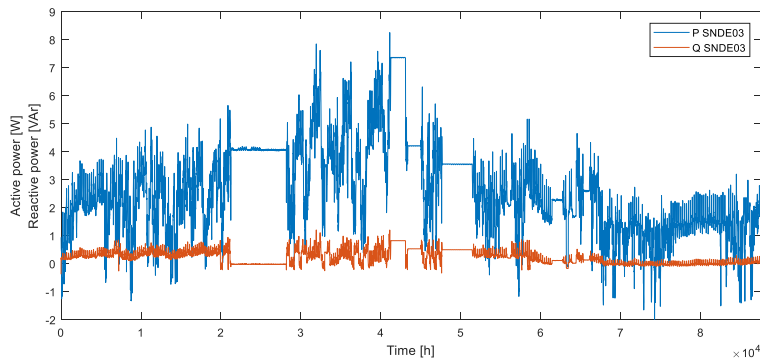


Figure 53. Active and reactive power flows at HV/MV connection point in Scenario 2018/2 offline when $T_s = 0.1$ s.

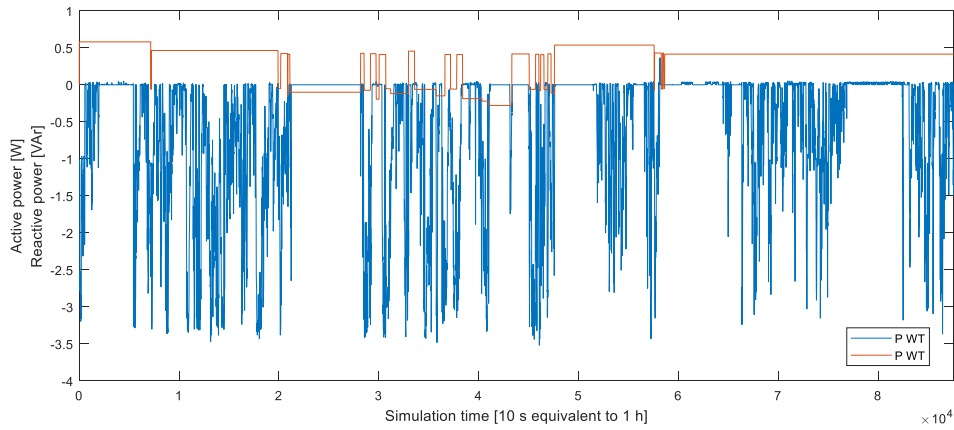


Figure 54. Active and reactive power of WT when input data was step type in Scenario 2018/2 offline when $T_s = 0.1$ s.

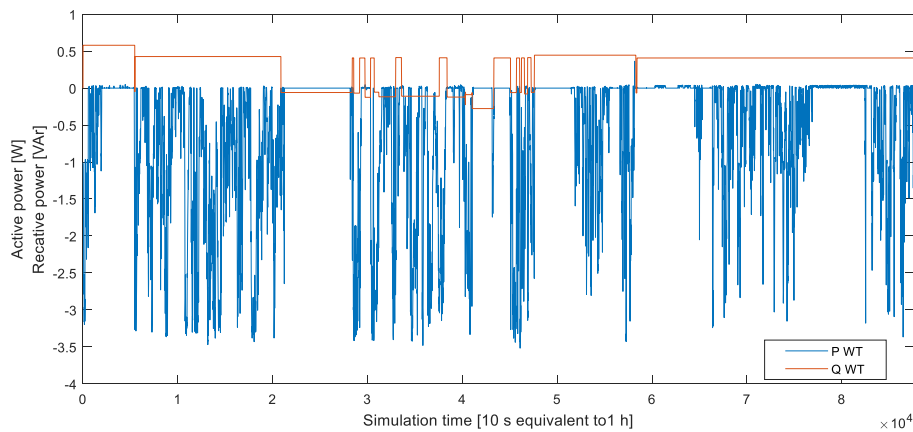


Figure 55. Active and reactive power of WT when input data was interpolated in Scenario 2018/2 of-line when $T_s = 0.1$ s.

5.2.3 Scenario 2028/1

In Figure 56 is presented the simulation results.

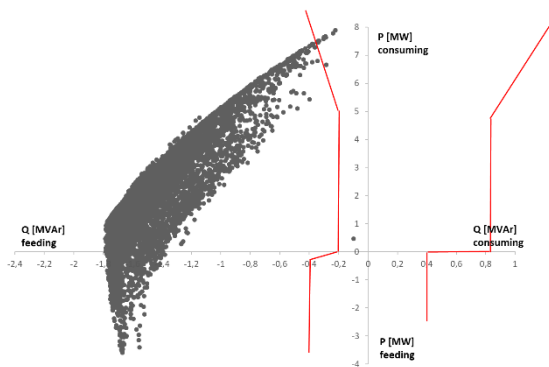


Figure 56. Reactive power window in Scenario 2028/1 offline when $T_s = 0.1$ s and input data was step function.

5.2.4 Scenario 2028/2 – SR

In Figure 57 is presented the simulation results.

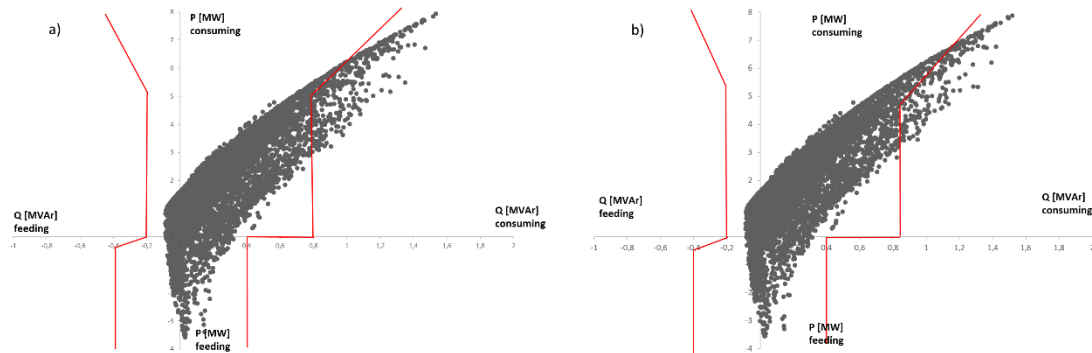


Figure 57. Reactive power window in Scenario 2028/2 offline when $T_s = 0.1$ s, input data was a) step function, b) interpolated and when SR was voltage dependent.

5.2.5 Scenario 2028/3 – SR and $\cos \varphi$ control of PV inverters

In Figure 58 is presented the simulation results.

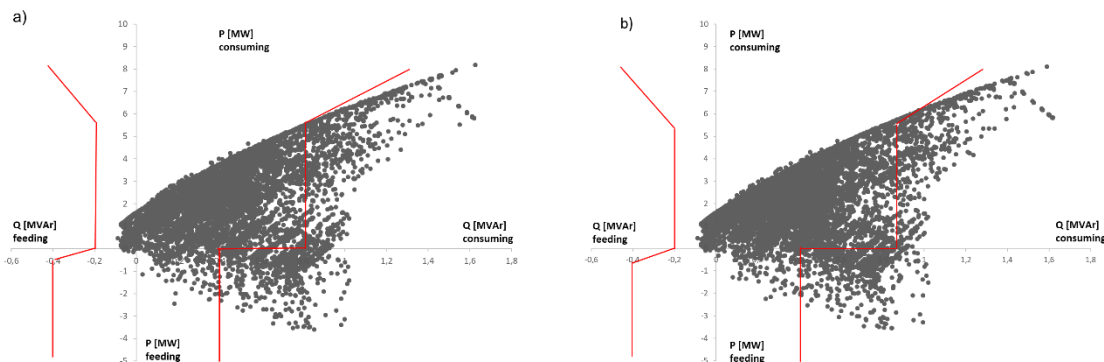


Figure 58. Reactive power window in Scenario 2028/3 offline when $T_s = 0.1$ s and input data was a) step function and b) interpolated.

5.2.6 Scenario 2028/4 – SR and RPW control of WT converter

This scenario was tested by different variations of set-ups; the input data was either step function or interpolated, the SR was either constant Q or voltage dependent, the limits for the RPW controller varied from TSO limits ± 0 , ± 50 to ± 100 kVar. In Figure 58 - Figure 63 is presented the simulation results.

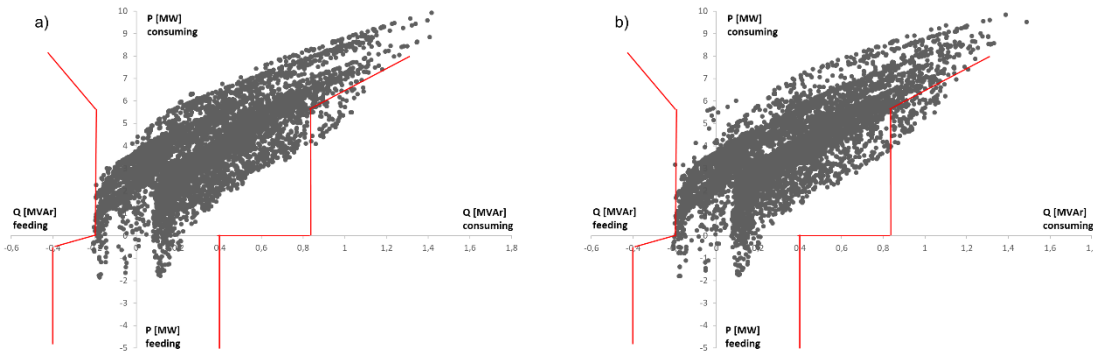


Figure 59. Reactive power window in Scenario 2028/4 offline when $T_s = 0.1$ s and input data was a) step function, b) interpolated. The shunt reactor Q was constant 1.75 MVar. The RPW controller was set up to the TSO limits.

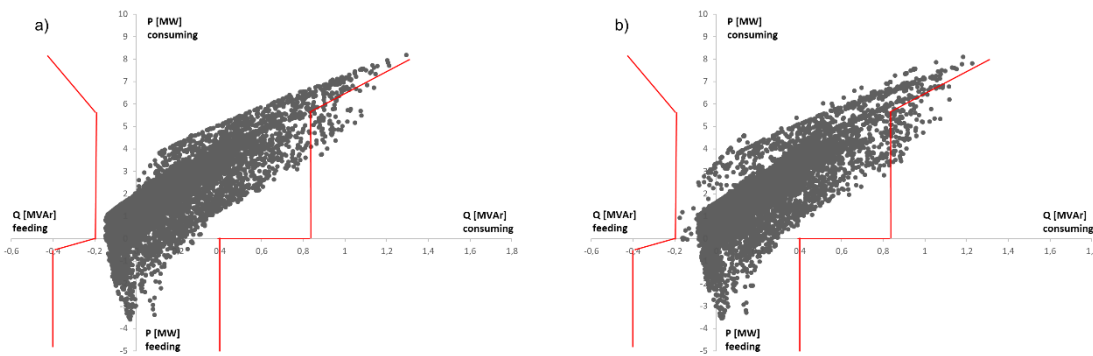


Figure 60. Reactive power window in Scenario 2028/4 offline when $T_s = 0.1$ s and input data was a) step function, b) interpolated. The shunt reactor was voltage dependent. The RPW controller was set up to the TSO limits.

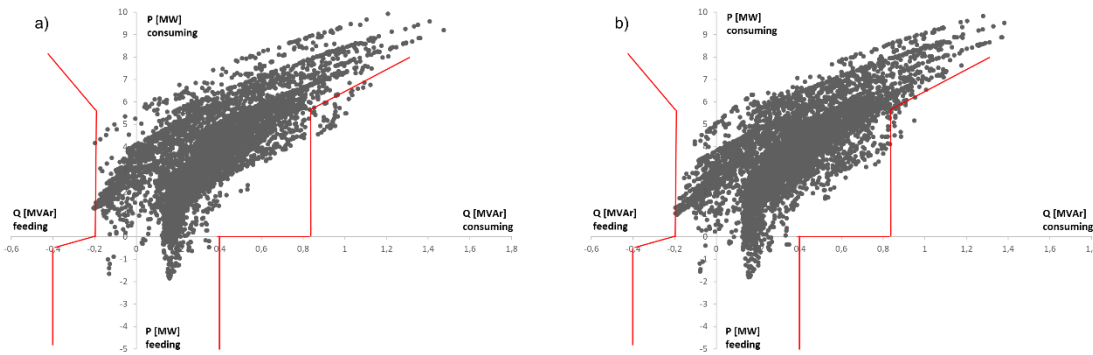


Figure 61. Reactive power window in Scenario 2028/4 offline when $T_s = 0.1$ s and input data was a) step function, b) interpolated. The shunt reactor Q was constant 1.75 MVar. The RPW controller was set up to the TSO limits +/- 50 kVar.

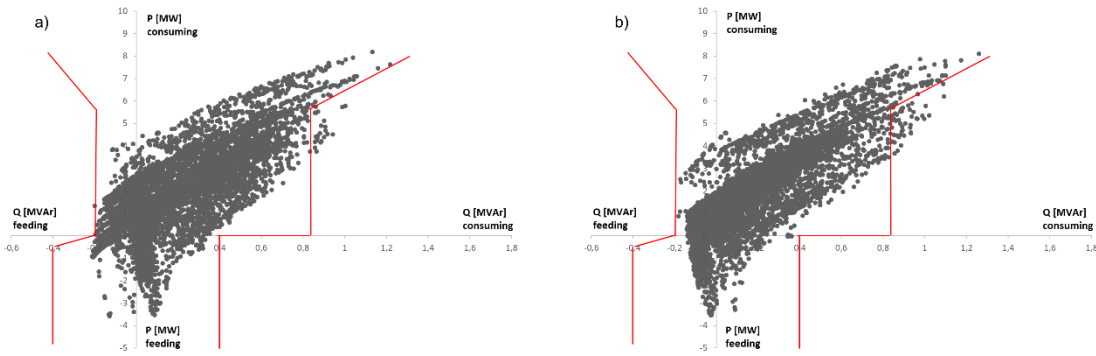


Figure 62. Reactive power window in Scenario 2028/4 offline when $T_s = 0.1$ s and input data was a) step function, b) interpolated. The shunt reactor Q was voltage dependent. The RPW controller was set up to the TSO limits ± 50 kVar.

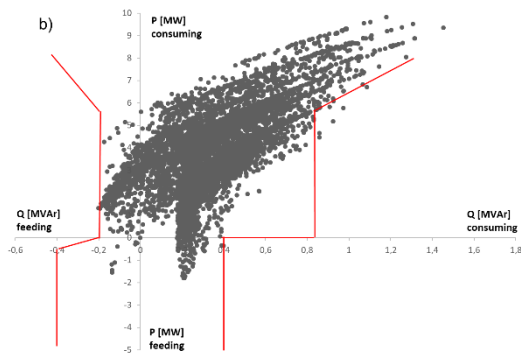


Figure 63. Reactive power window in Scenario 2028/4 offline when $T_s = 0.1$ s and input data interpolated. The shunt reactor Q was constant 1.75 MVar. The RPW controller was set up to the TSO limits ± 100 kVar.

5.3 Real-time simulations

The real-time simulations were performed for SIL and CHIL for Scenarios 2018/2 and 2028/2 with different control parameter setups and different input data reading cycles. The HW for CHIL simulations were Beagle Bone Black (BBB) as well as FPGA.

5.3.1 Software in the loop simulations

5.3.1.1 Scenario 2018/2 – TSO limits

The first simulation was performed in the situation where the limits of the RPW controller were set-up according to the TSO limits. The time-step for input data reading was set to $T_s = 1$ s and 0.1 s. The reactive power of the WT converter is presented in Figure 64 when $T_s = 1$ s, and when the input data was step function. The reactive power of the wind turbine converter is presented in Figure 65 and Figure 66 when $T_s = 0.1$ s, and when the input data was step function or interpolated data respectively. The reactive power window is presented in Figure 67.

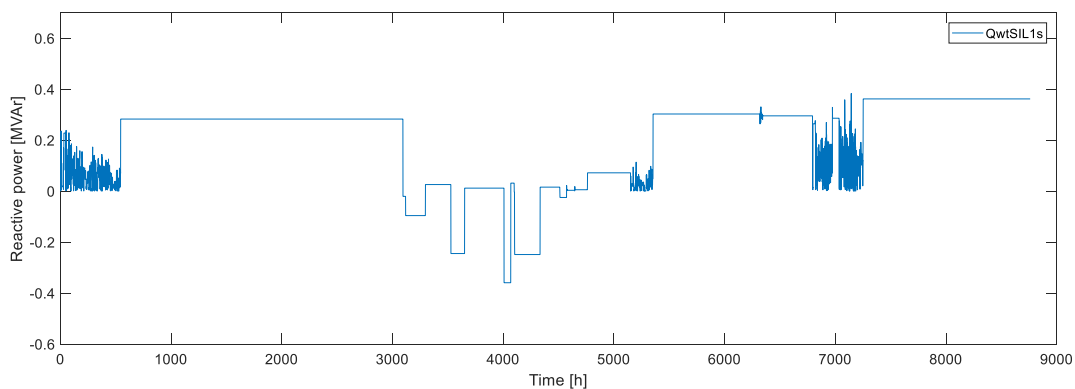


Figure 64. Reactive power of the WT converter in Scenario 2018/2 SIL, when $T_s = 1$ s, input data was step function and RPW control was set up to TSO limits.

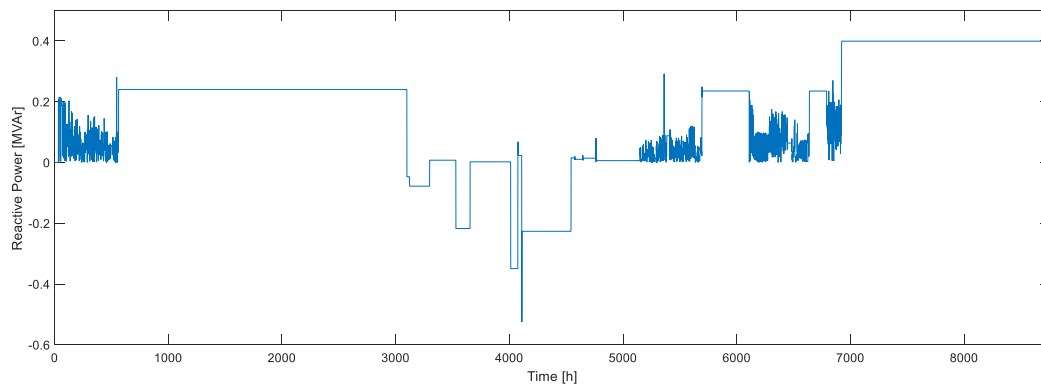


Figure 65. Reactive power of the WT converter in Scenario 2018/2 SIL, when $T_s = 0.1$ s, input data was step function and RPW control was set up to TSO limits.

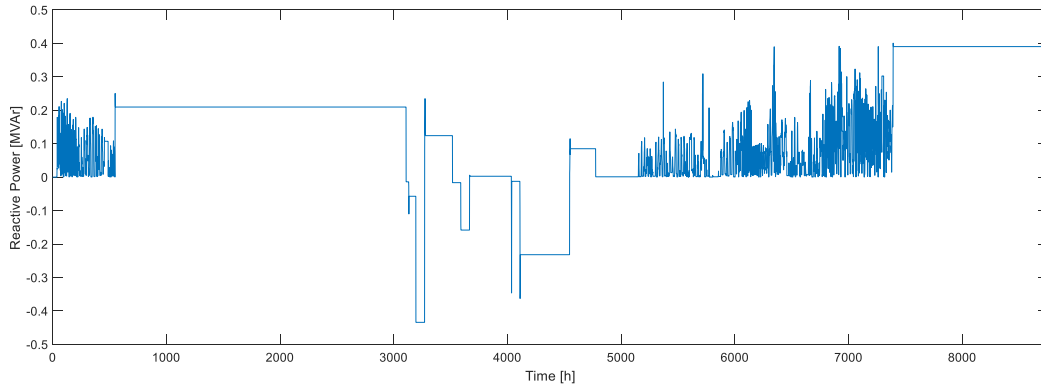


Figure 66. Reactive power of the WT converter in Scenario 2018/2 SIL, when $T_s = 0.1$ s, input data was interpolated and RPW control was set up to TSO limits.

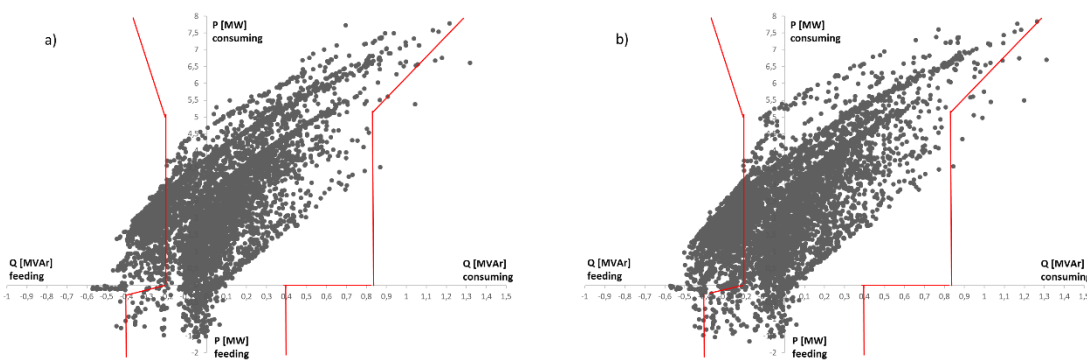


Figure 67. Reactive power window in Scenario 2018/2 SIL when $T_s = 0.1$ s and input data was a) step function, b) interpolated. The RPW controller was set up to the TSO limits.

5.3.1.2 Scenario 2018/2 – TSO limits ± 50 kVar

The second simulation case was performed in the situation where the RPW controller limits were set-up for TSO limits ± 50 kVar. The time-step for input data reading was set to $T_s = 1$ s and 0.1 s. The reactive power of the WT converter is presented in the Figure 68 and Figure 69 when $T_s = 1$ s. It can be noticed that the system is stable and the control of the converter is peaceful. The reactive power windows are presented in Figure 70. The reactive power of the WT converter is presented in Figure 71 and Figure 72 when $T_s = 0.1$ s. It can be noticed that the system is stable and the control of the converter is peaceful. The reactive power windows are presented in Figure 73.

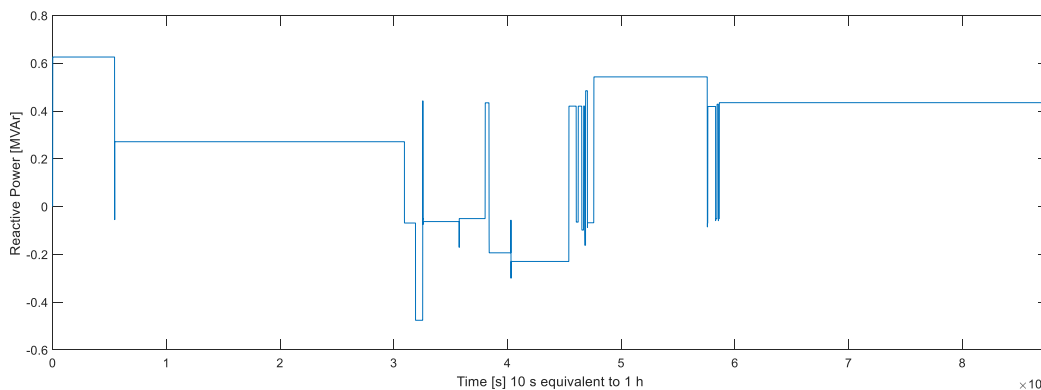


Figure 68. Reactive power of the WT converter in Scenario 2018/2 SIL, when $T_s = 1$ s, input data was step function and RPW control was set up to TSO limits ± 50 kVar.

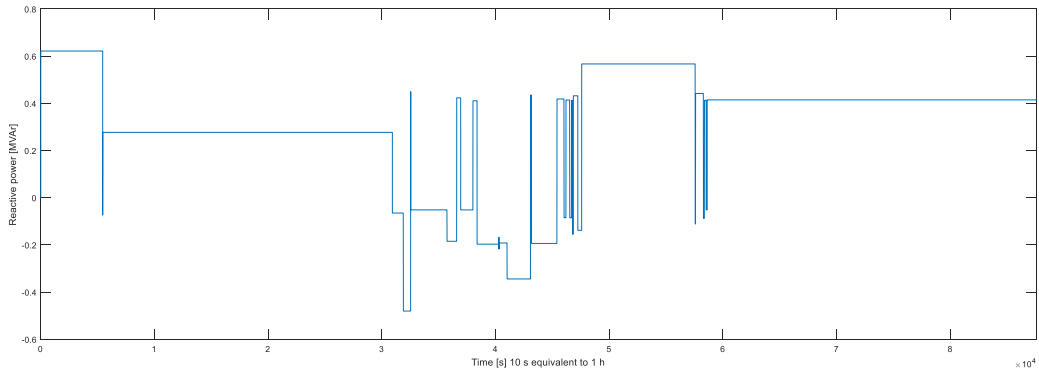


Figure 69. Reactive power of the WT converter in Scenario 2018/2 SIL, when $T_s = 1$ s, input data was interpolated and RPW control was set up to TSO limits ± 50 kVAr.

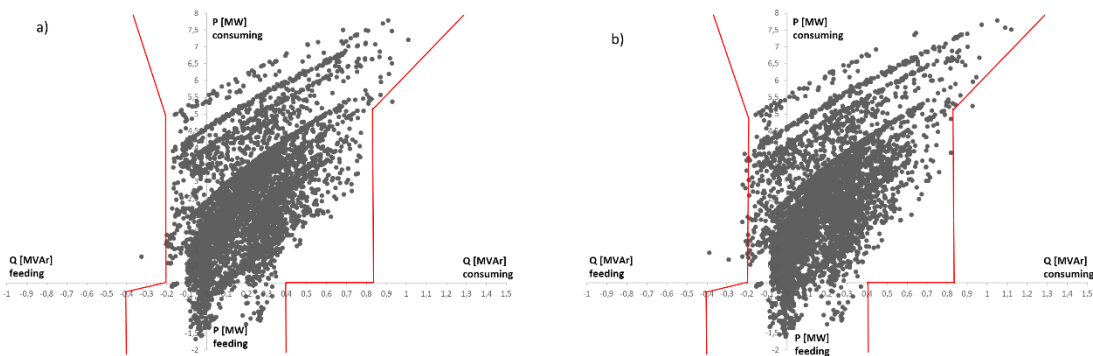


Figure 70. Reactive power window in Scenario 2018/2 SIL when $T_s = 1$ s and input data was a) step function, b) interpolated. The RPW controller was set up to the TSO limits ± 50 kVAr.

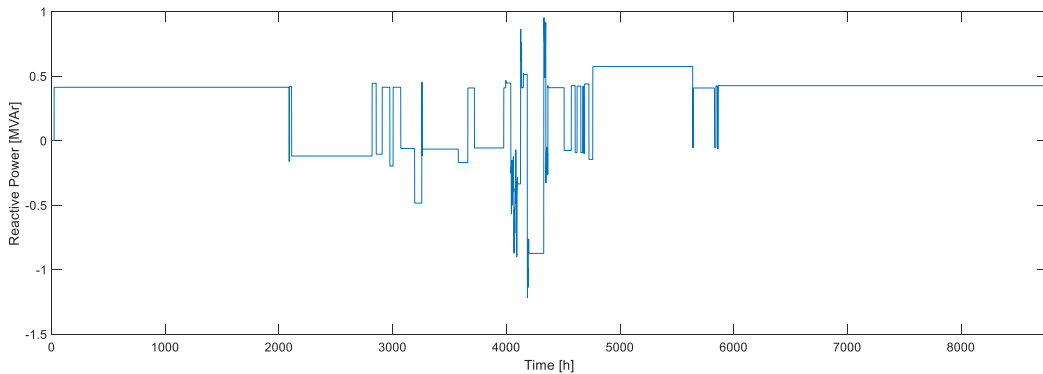


Figure 71. Reactive power of the WT converter in Scenario 2018/2 SIL, when $T_s = 0.1$ s, input data was step function and RPW control was set up to TSO limits ± 50 kVAr.

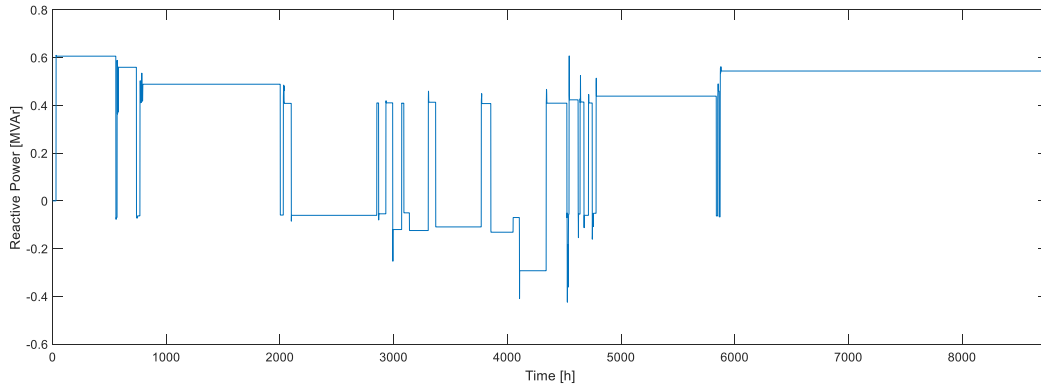


Figure 72. Reactive power of the WT converter in Scenario 2018/2 SIL, when $T_s = 0.1$ s, input data was interpolated and RPW control was set up to TSO limits ± 50 kVar.

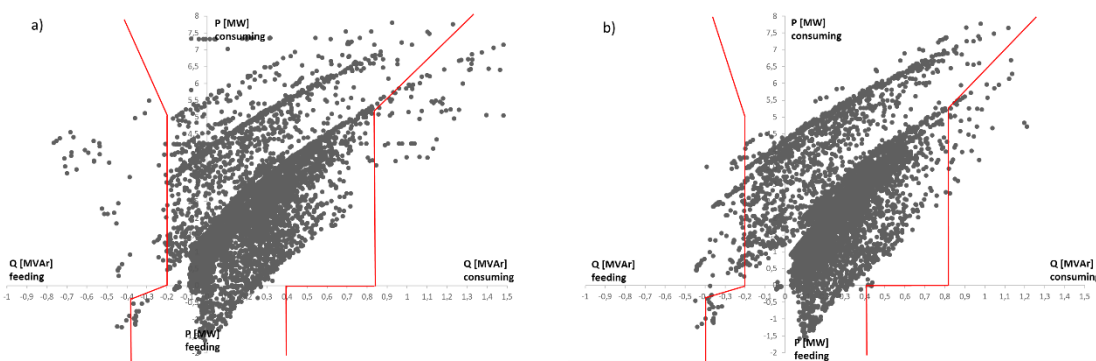


Figure 73. Reactive power window in Scenario 2018/2 SIL when $T_s = 0.1$ s and input data was a) step function, b) interpolated. The RPW controller was set up to the TSO limits ± 50 kVar.

5.3.1.3 Scenario 2018/2 – TSO limits ± 100 kVar

The third simulation case was performed in the situation where the RPW controller limits were set-up for TSO limits ± 100 kVar. The time-step for input data reading was set to 0.1 s. The reactive power of the WT converter is presented in Figure 74 and in Figure 75.

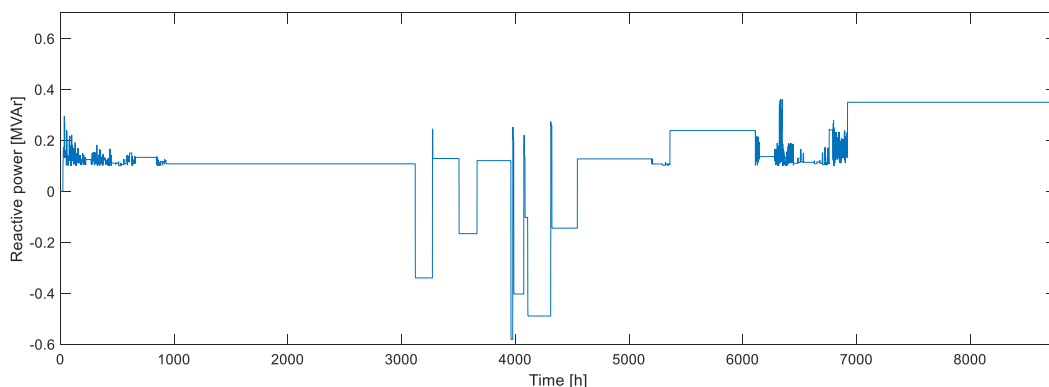


Figure 74. Reactive power of the WT converter in Scenario 2018/2 SIL, when $T_s = 0.1$ s, input data was step function and RPW control was set up to TSO limits ± 100 kVar.

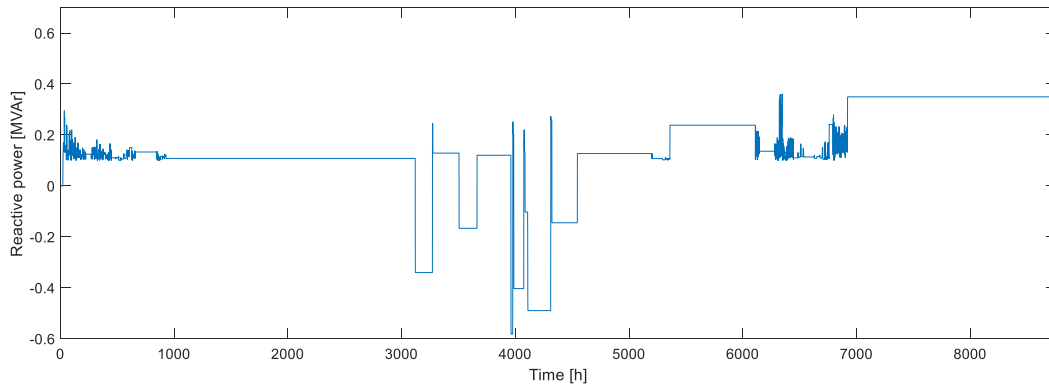


Figure 75. Reactive power of the WT converter in Scenario 2018/2 SIL, when when $T_s = 0.1$ s, input data was interpolated and RPW control was set up to TSO limits ± 100 kVAr.

5.3.2 Controller hardware in the loop simulations

In the Table 6 is presented the performed CHIL tests, which were carried out with BBB as well as with FPGA.

Table 6. Tests carried out as CHIL.

Test n:o	HW	Timescale	2018		2028		
			TSO limits	TSO tuned limits (± 50 kVAr)	TSO limits	TSO tuned limits (± 50 kVAr)	TSO tuned limits (± 100 kVAr)
Test 1	BBB	1 s		X			
Test 2	BBB	0.1 s		X			
Test 3	BBB	0.1 s	X				
Test 4	FPGA	0.1 s		X			
Test 5	FPGA	0.1 s	X				
Test 6	FPGA	1 s	X				
Test 7	FPGA	0.1 s			X		
Test 8	FPGA	0.1 s				X	
Test 9	FPGA	0.1 s					X
Test 10	BBB	0.1 s			X		
Test 11	BBB	0.1 s				X	
Test 12	BBB	0.1 s					X
Test 13	BBB	1 s	X				

5.3.2.1 CHIL test results

In the following Figure 76 - Figure 88 the test results of controlled reactive power are presented.

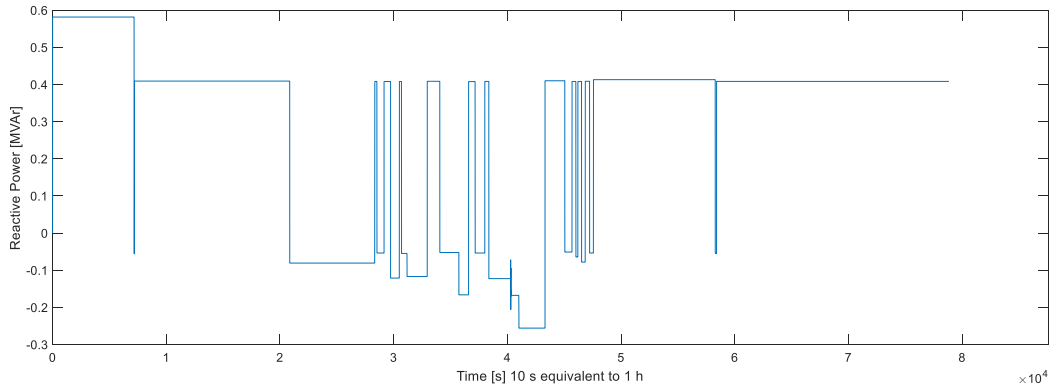


Figure 76. Test 1. Reactive power of the WT converter in Scenario 2018/2 CHIL (BBB), when $T_s = 1$ s, input data was step function and RPW control was set up to TSO limits ± 50 kVar.

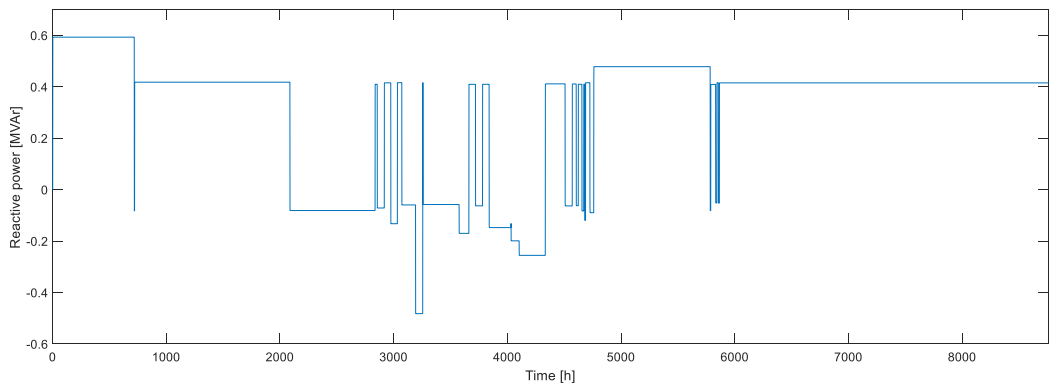


Figure 77. Test 2. Reactive power of the WT converter in Scenario 2018/2 CHIL (BBB), when $T_s = 0.1$ s, input data was step function and RPW control was set up to TSO limits ± 50 kVar.

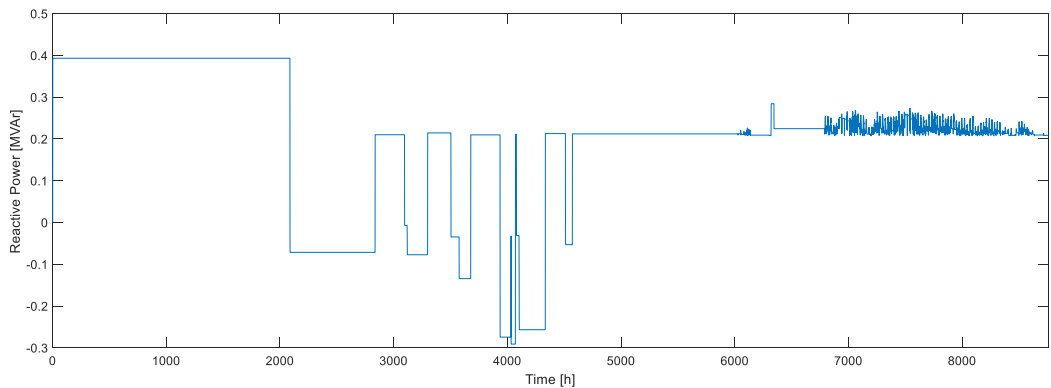


Figure 78. Test 3. Reactive power of the WT converter in Scenario 2018/2 CHIL (BBB), when $T_s = 0.1$ s, input data was step function and RPW control was set up to TSO limits.

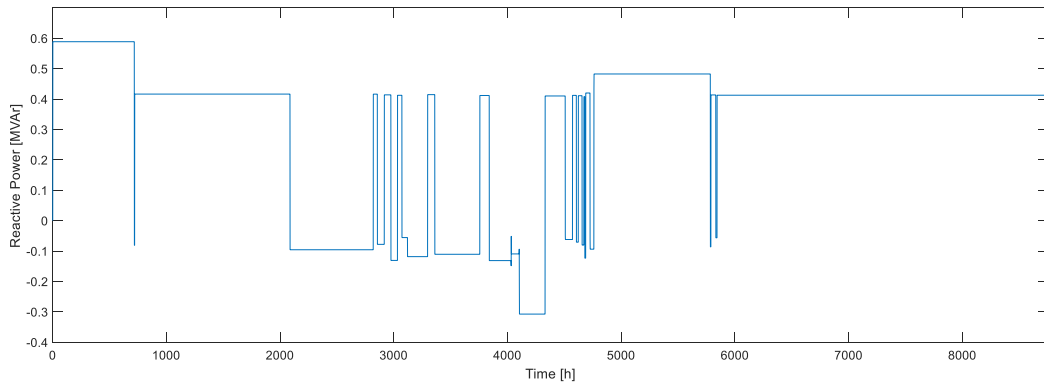


Figure 79. Test 4. Reactive power of the WT converter in Scenario 2018/2 CHIL (FPGA), when $T_s = 0.1$ s, input data was step function and RPW control was set up to TSO limits ± 50 kVAr.

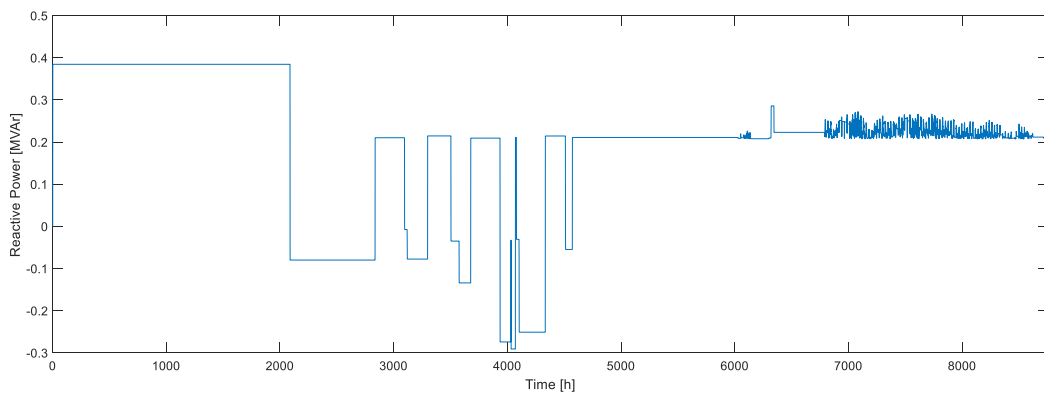


Figure 80. Test 5. Reactive power of the WT converter in Scenario 2018/2 CHIL (FPGA), when $T_s = 0.1$ s, input data was step function and RPW control was set up to TSO limits.

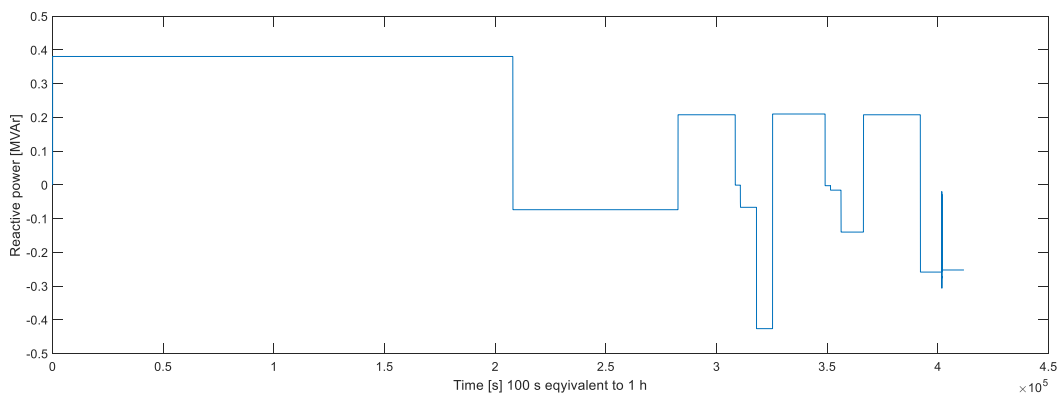


Figure 81. Test 6. Reactive power of the WT converter in Scenario 2018/2 CHIL (FPGA), when $T_s = 1$ s, input data was step function and RPW control was set up to TSO limits.

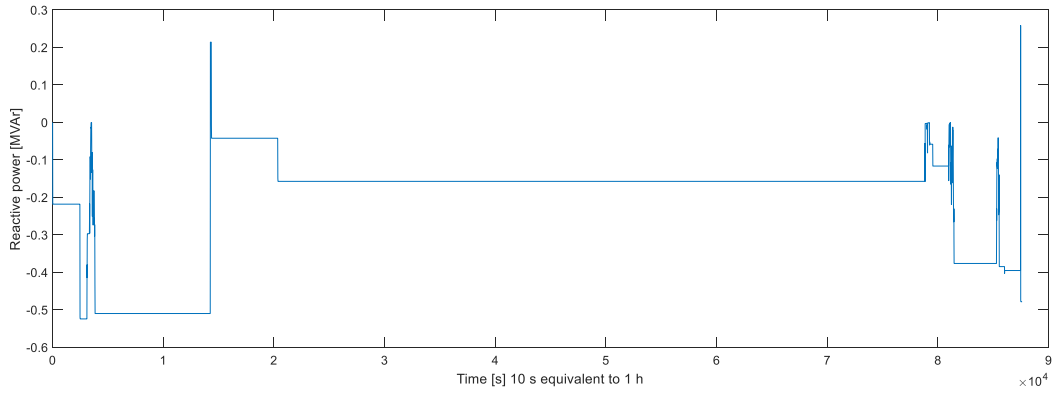


Figure 82. Test 7. Reactive power of the WT converter in Scenario 2028/2 CHIL (FPGA), when $T_s = 0.1$ s, input data was step function and RPW control was set up to TSO limits.

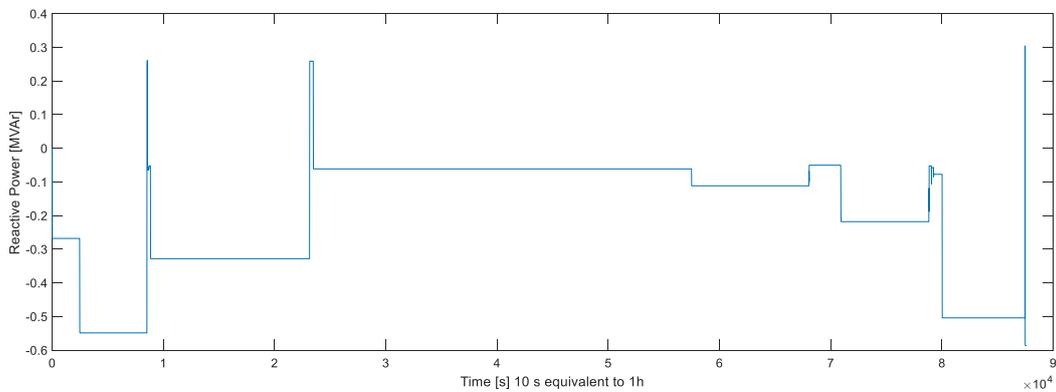


Figure 83. Test 8. Reactive power of the WT converter in Scenario 2028/2 CHIL (FPGA), when $T_s = 0.1$ s, input data was step function and RPW control was set up to TSO limits ± 50 kVAR.

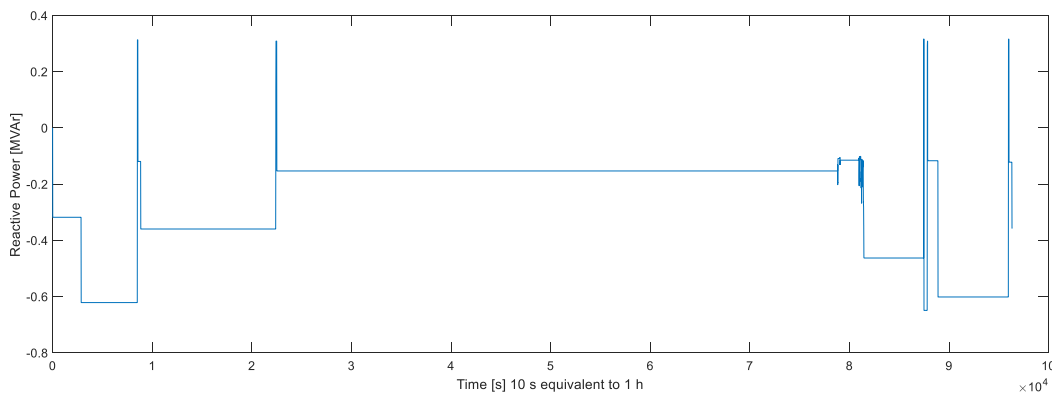


Figure 84. Test 9. Reactive power of the WT converter in Scenario 2028/2 CHIL (FPGA), when $T_s = 0.1$ s, input data was step function and RPW control was set up to TSO limits ± 100 kVAR.

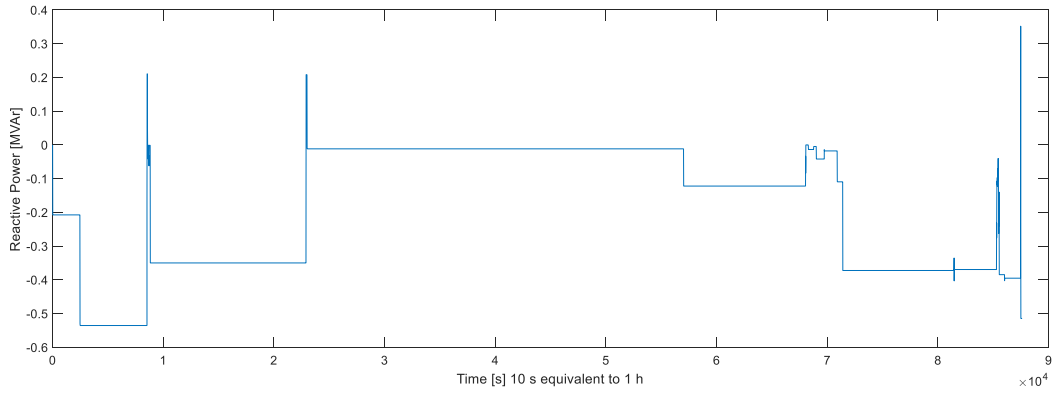


Figure 85. Test 10. Reactive power of the WT converter in Scenario 2028/2 CHIL (BBB), when $T_s = 0.1$ s, input data was step function and RPW control was set up to TSO limits.

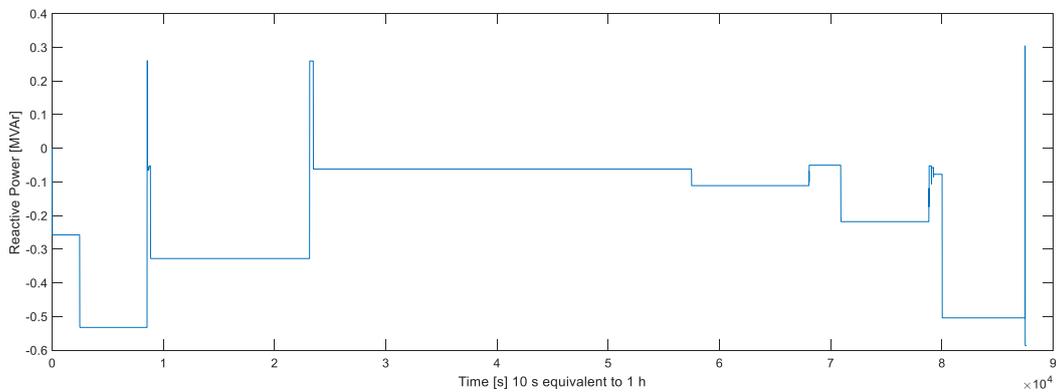


Figure 86. Test 11. Reactive power of the WT converter in Scenario 2028/2 CHIL (BBB), when $T_s = 0.1$ s, input data was step function and RPW control was set up to TSO limits ± 50 kVAR.

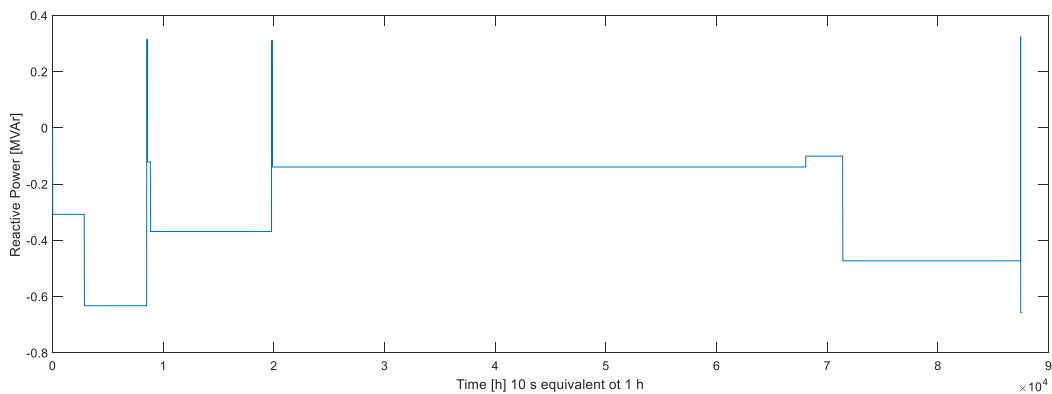


Figure 87. Test 12. Reactive power of the WT converter in Scenario 2028/2 CHIL (BBB), when $T_s = 0.1$ s, input data was step function and RPW control was set up to TSO limits ± 100 kVAR.

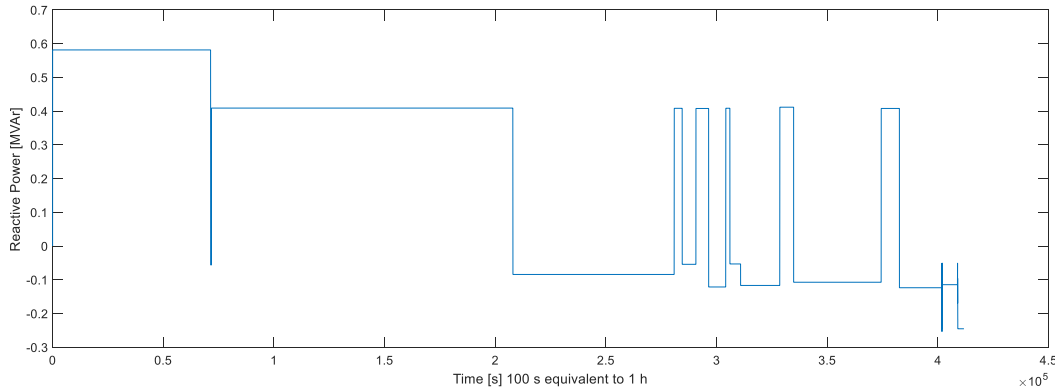


Figure 88. Test 13. Reactive power of the WT converter in Scenario 2018/2 CHIL (BBB), when $T_s = 1$ s, input data was step function and RPW control was set up to TSO limits.

5.3.3 The round trip Goose latency

The round trip GOOSE latency was calculated for the overall completed tests. The main objective within the measuring task was to verify that the performance of the DUT for publishing of the GOOSE messages was compliant with the IEC 61850 (not exceed 4ms). Moreover, to verify that the DUT has the ability to operate within the multi-vendor environment ensuring the interoperability concept. Finally, measured latency of the GOOSE messages was compared among IEDs from different designed light-weight IEDs.

Using a Normal Distribution probability density function the mean of the round trip GOOSE messages from the SPS model and different IEDs were measured and calculated. These measurements are involved seven individual times in which that may affect the connection channel performance as illustrated in (1)

$$\bar{t}_{RT} = \bar{t}_{out.TS} + \bar{t}_{net} + \bar{t}_{in.DUT} + \bar{t}_{App} + \bar{t}_{out.DUT} + \bar{t}_{net} + \bar{t}_{in.TS} \quad (1)$$

where \bar{t}_{RT} is the mean round trip time, $\bar{t}_{out.TS}$, and $\bar{t}_{in.TS}$ are the mean times in and out for the client IED (test system) that attempts to connect to the server. $\bar{t}_{in.DUT}$, and $\bar{t}_{out.DUT}$ are the mean times in and out for the device under test (DUT), \bar{t}_{App} is the application mean time within the DUT.

In the Figure 89 is presented the round trip GOOSE latency for the BBB and for the FPGA. The mean the round trip latency calculation based on (1) was for BBB 4.548406 ms and for FPGA 2.384781 ms. From the achieved results, it is obviously clear that the FPGA is more promising instrument with less round trip latency (2.3ms) in which that could better be used for the smart grid/microgrid central controller SGCC/MGCC. The less round trip latency for the FPGA is expected since it has 925 MHz, A Dual-Core ARM Cortex™-A9, 10/100/1000 Mbps Ethernet with the high-speed busses to exchange data between the hard processor system (HPS) and FPGA. Whereas the BBB has AM335x 1GHz ARM® Cortex-A8, 10/100 Mbps Ethernet. In the Figure 90 is presented the GOOSE messages processing time in both devices in microseconds.

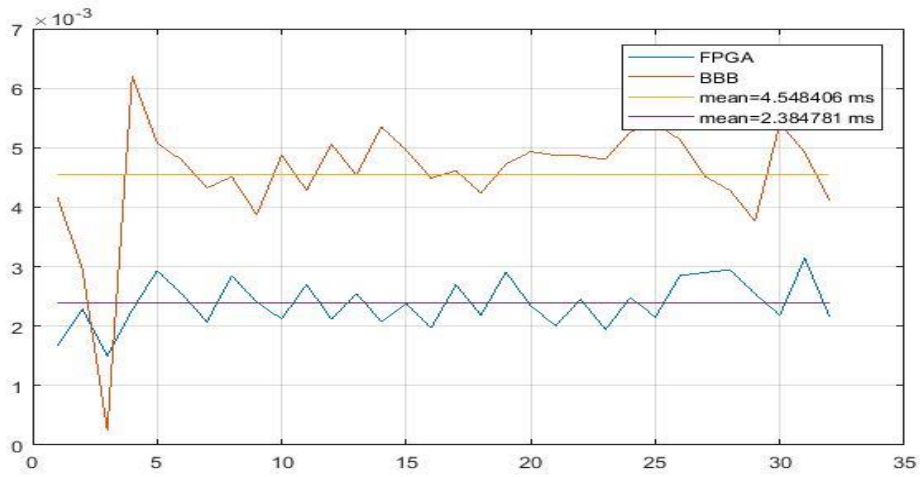


Figure 89. GOOSE round trip latency for the BBB and FPGA.

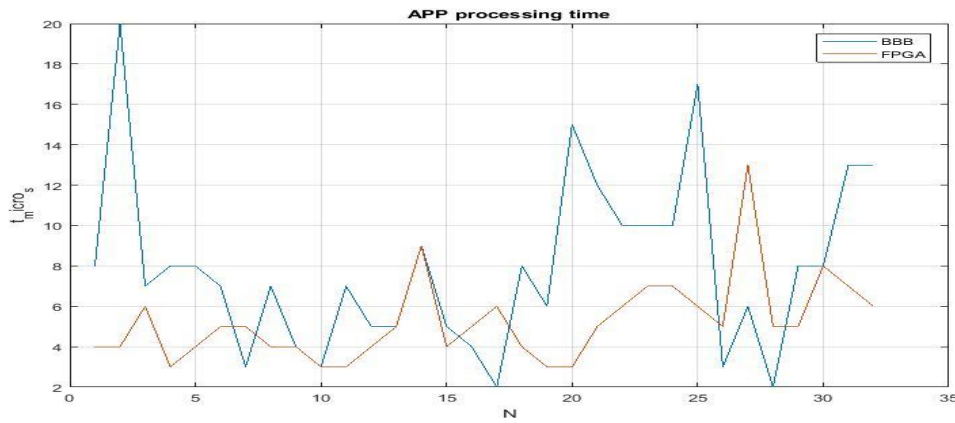


Figure 90. BBB and FPGA GOOSE message processing time.

5.3.4 Comparison of the different simulations

Comparison were made for SIL and CHIL simulations.

5.3.4.1 Comparison in Scenario 2018/2 with TSO ± 50 kVAr limits

The comparison in Scenario 2018/2 is done between SIL, BBB (Test 2) and FPGA (Test 4). In Figure 91 is presented reactive power from the WT converter when the controller was BBB or FPGA. In Figure 92 is presented reactive power from the WT converter when the controller was SIL or BBB. In Figure 93 is presented reactive power from the WT converter when the controller was SIL or FPGA. It can be noticed that the BBB cannot perform so well than FPGA, in turn the FPGA performs as well as SIL.

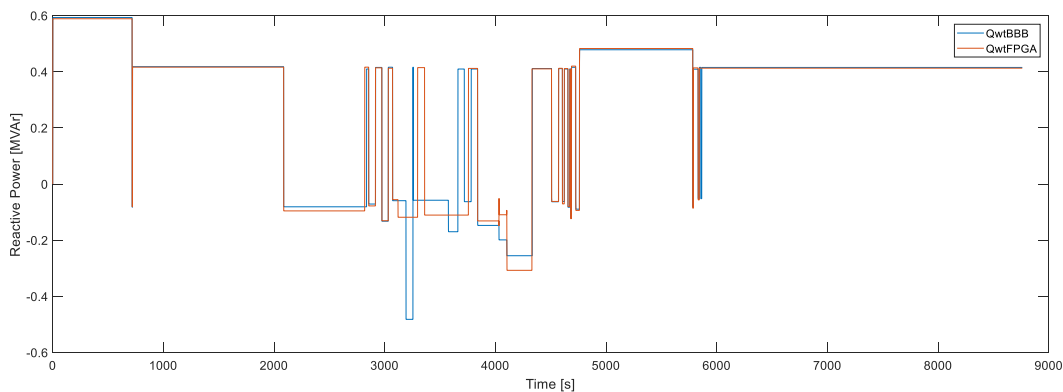


Figure 91. Reactive power of the WT converter in Scenario 2018/2 CHIL BBB and FPGA, when $T_s = 0.1$ s, input data was step function and RPW control was set up to TSO limits ± 50 kVAr, except QD1 limit to -0.2 MVar.

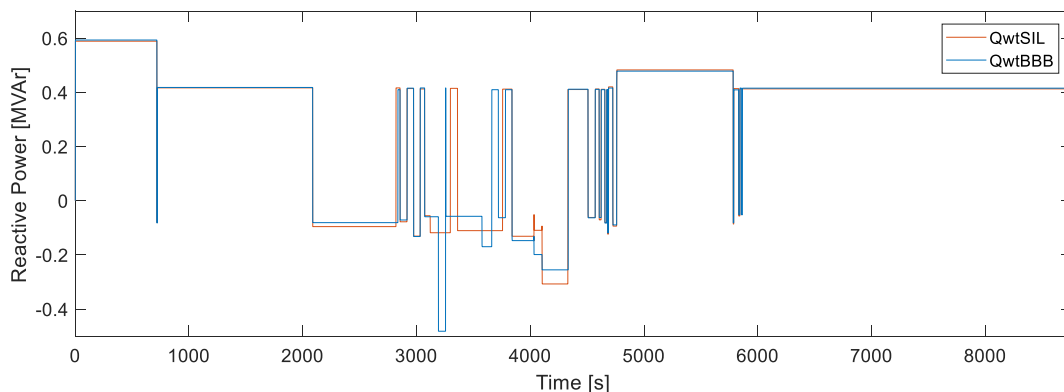


Figure 92. Reactive power of the WT converter in Scenario 2018/2 SIL and CHIL BBB, when $T_s = 0.1$ s, input data was step function and RPW control was set up to TSO limits ± 50 kVAr, except QD1 limit to -0.2 MVar.

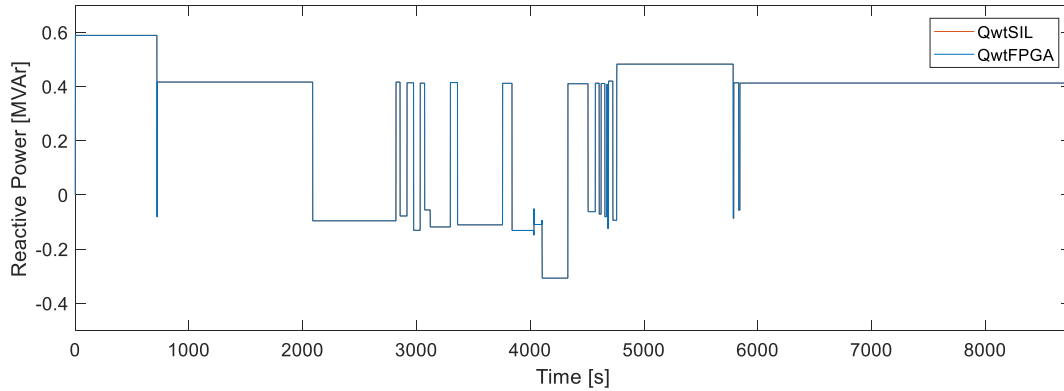


Figure 93. Reactive power of the WT converter in Scenario 2018/2 SIL and CHIL FPGA, when $T_s = 0.1$ s, input data was step function and RPW control was set up to TSO limits ± 50 kVAr, except QD1 limit to -0.2 MVar.

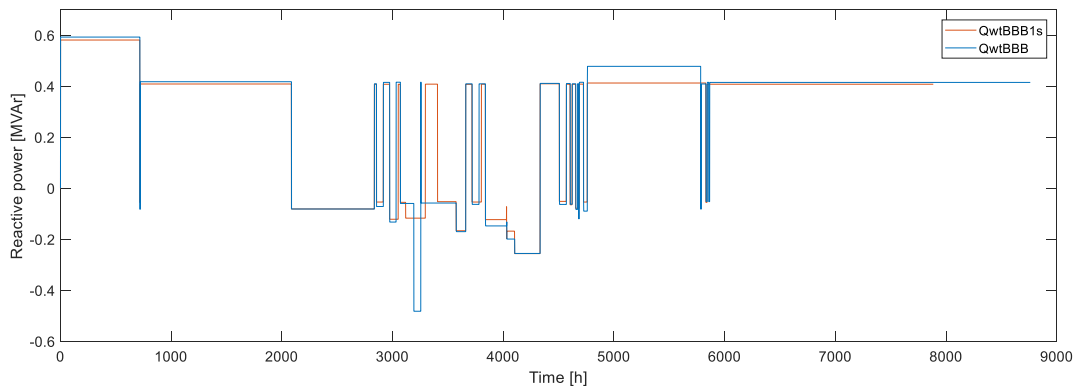


Figure 94. Reactive power of the WT converter in Scenario 2018/2 BBB when $T_s = 0.1$ s and BBB when $T_s = 1$ s, input data was step function and RPW control was set up to TSO limits ± 50 kVAr, except QD1 limit to -0.2 MVar.

5.3.4.2 Comparison in Scenario 2018/2 with TSO limits

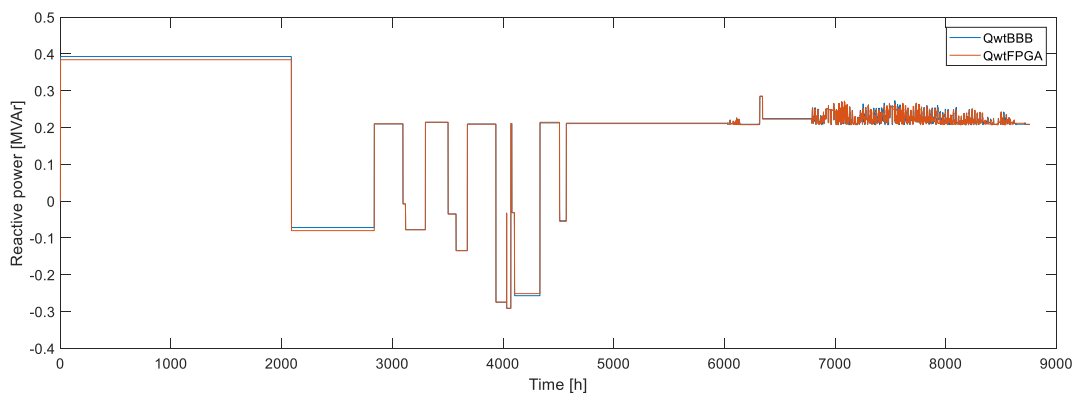


Figure 95. Reactive power of the WT converter in Scenario 2018/2 CHIL BBB and FPGA, when $T_s = 0.1$ s, input data was step function and RPW control was set up according to TSO limits except QD1 limit to 0.

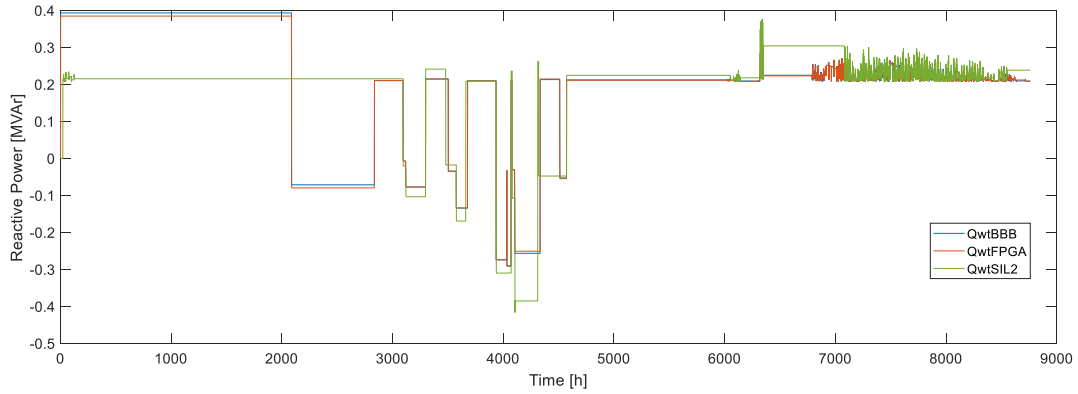


Figure 96. Reactive power of the WT converter in Scenario 2018/2 CHIL BBB and FPGA as well as SIL, when $T_s = 0.1$ s, input data was step function and RPW control was set up according to TSO limits except QD1 limit to 0.

5.3.4.3 Comparison in Scenario 2028/2 with TSO ± 50 kVAr limits

This is comparison between Test 8 and Test 11.

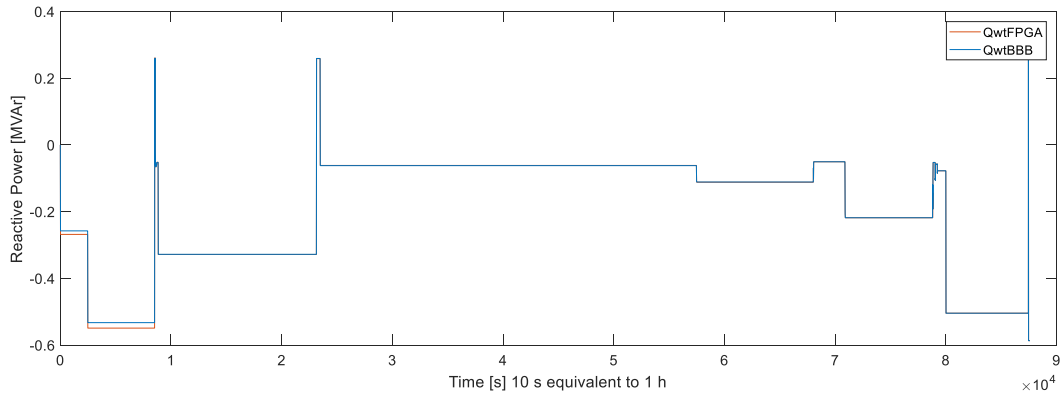


Figure 97. Reactive power of the WT converter in Scenario 2018/2 CHIL BBB and FPGA, when $T_s = 0.1$ s, input data was interpolated and RPW control was set up according to TSO limits ± 50 kVAr.

5.3.4.4 Comparison in Scenario 2028/2 with TSO limits

This is comparison between Test 7 and Test 10.

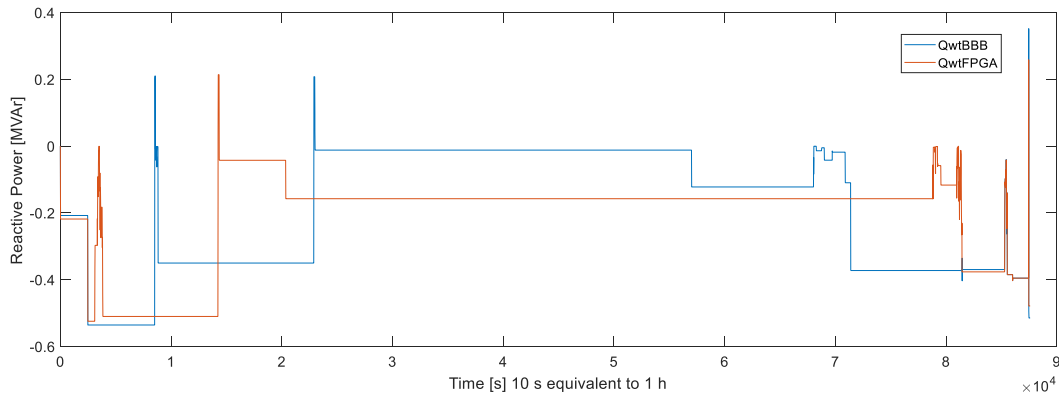


Figure 98. Reactive power of the WT converter in Scenario 2018/2 CHIL BBB and FPGA, when $T_s = 0.1$ s, input data was interpolated and RPW control was set up according to TSO limits, except QD1 limit to 0.

6 Open Issues and Suggestions for Improvements

For further studies of Volt/Var management:

- an OLTC should be modelled
- different scenarios of reactive power control with PV inverters
 - NDZ
 - $Q(U)$
 - $\cos\phi(P)$

As the CHIL test results showed, the FPGA was more reliable than the BBB to perform the tests. For further studies, when aiming CHIL tests, FPGA is preferable.

The RPW controller should be predictive in order that (Q, P) points would stay inside the window reliably. Now the adaptive control followed the measurements and made a decision about a new set point if needed. So to say the control was all the time “late”. Next, a predictive tool should be implemented to the RPW control.

7 Dissemination Planning

The results will be presented as scientific publications and will be attached to Katja Sirviö's doctoral thesis. The publications will be conference paper and a journal paper. The conference paper will comprise of the development and testing of the RT co-simulation platform in collaboration with host Lab. A possible conference could be ISGT Europe 2019. The journal paper will contain the results of the developed simulation cases, U/Q controller as SIL and CHIL for technical AS in the SSG case. The project has been presented in a one-day international workshop in OFFIS on "Resilience and security in digitalized energy system" in September 2018. University of Vaasa and Offis Institute for Information Technology could get benefits from the developed RT smart grid simulation platform for future research and collaboration.

8 References

- [1] „IEEE Standard for the Specification of Microgrid Controllers,“ *IEEE Std 2030.7-2017*, pp. 1-43, 2018.
- [2] „IEEE Standard for the Testing of Microgrid Controllers,“ *IEEE 2030.8-2018*, pp. 1-42, 2018.
- [3] EU, Network Code on Demand Connection, Commission Regulation (EU) 2016/1388, 2016.
- [4] EU, Network Code on Requirements for Grid Connected Generators, Commission Regulation (EU) 2016/631, 2016.
- [5] Fingrid, „Supply of Reactive Power and Maintenance of Reactive Power Reserves,“ 2017. [Online]. Available: https://www.fingrid.fi/globalassets/dokumentit/en/customers/grid-connection/supply-of-reactive-power-and-maintenance-of-reactive-power-reserves_2017.pdf.
- [6] H. Laaksonen und P. Hovila, „Flexzone concept to enable resilient distribution grids - Possibilities in Sundom Smart Grid,“ in *CIREC Worksop*, Helsinki, 2016.
- [7] H. Laaksonen und P. Hovila, „Future-proof islanding detection schemes in SundomSmart Grid,“ in *CIREC Conference on Electricity Distribution*, Glasgow, 2017.
- [8] S. Uebermasser, C. Groiss, A. Einfalt, N. Thie, M. Vasconcelos, J. Helguero, H. Laaksonen und P. Hovila, „Requirements for coordinated ancillary services covering different voltage levels,“ in *CIREC Conference on Electricity Distribution*, Glasgow, 2017.
- [9] H. Laaksonen, P. Hovila und K. Kauhaniemi, „Combined islanding detection scheme utilizing active network management for future resilient distribution networks,“ in *The 14th International Conference on Developments in Power System Protection (DPSP)*, Belfast, 2018.
- [10] K. Sirviö, L. Välikkilä, H. Laaksonen, K. Kauhaniemi und A. Rajala, „Prospects and Costs for Reactive Power Control in Sundom Smart Grid,“ in *IEEE PES Innovative Smart Grid Technologies Conference Europe , ISGT Europe*, Sarajevo, 2018.
- [11] A. Isaacs, „Simulation Technology: The Evolution of the Power System Network,“ *IEEE Power and Energy Magazine*, Bd. 15, Nr. 4, pp. 88-102, 2017.
- [12] P. Palensky, E. Widl und A. Elsheikh, „Simulating Cyber-Physical Energy Systems: Challenges,“ *IEEE Transactions on Systems, Man, and Cybernetics: Systems*, Bd. 44, Nr. 3, pp. 318-326, 2014.
- [13] D. Babazadeh, *Co-simulation in Energy Domain -Definition and Application*, 2017.
- [14] F. Schloegl, S. Rohjans, S. Lehnhoff, J. Velasquez, C. Steinbrink und P. Palensky, „Towards a classification scheme for co-simulation approaches in energy systems,“ in *2015 International Symposium on Smart Electric Distribution Systems and Technologies (EDST)*, Vienna, 2015.
- [15] C. Rehtanz und X. Gillaud, „Real-time and co-simulations for the development of power system monitoring, control and protection,“ in *2016 Power Systems Computation Conference (PSCC)*, 2016.
- [16] S. N. C. B. H. Bhaskara, „Microgrids — A review of modeling, control, protection, simulation and future potential,“ in *2012 IEEE Power and Energy Society General Meeting*, San Diego, 2012.
- [17] D. Ton und J. Reilly, „Microgrid Controller Initiatives: An Overview of R&D by the U.S. Department of Energy,“ *IEEE Power and Energy Magazine*, pp. 24-31, July-Aug 2017.
- [18] A. Maitra und e. al., „Microgrid Controllers : Expanding Their Role and Evaluating Their Performance,“ *IEEE Power and Energy Magazine*, pp. 41-49, July-Aug 2017.

9 Annex

9.1 List of Figures

Figure 1. Product sales and standards cycle.....	9
Figure 2. On-line diagram of Sundom Smart Grid living lab.....	10
Figure 3. On-line diagram of Sundom Smart Grid living lab. [10].....	12
Figure 4. The outline of the simulated network.....	13
Figure 5. The simulation architecture in SM_block for SIL of reactive power control in SSG Status 2018. ...	14
Figure 6. The past, present and future of simulations. [13].....	15
Figure 7. Distributed DMS IEDs overall concept.....	17
Figure 8. Distributed DMS IEDs setup platform and gose round trip concept.....	18
Figure 9. Outline of the developed real-time co-simulation environment.....	23
Figure 10. Measured load at J06 Sulva feeder.....	24
Figure 11. Measured load at J07 Sundom feeder.....	24
Figure 12. Measured load at J09 Vaskiluoto feeder.....	25
Figure 13. Measured wind power generation.....	25
Figure 14. Simulated PV generation for Sundom school PV unit.....	25
Figure 15. Simulated and measured active power flows at 21 kV bus in Sundom Smart Grid.....	26
Figure 16. Simulated and measured reactive power flows at 21 kV bus in Sundom Smart Grid. Power factor of loads was set up 0.995 _{ind}	26
Figure 17. Voltage in 110 kV and 21 kV bus in Scenario 2018/1.....	26
Figure 18. Voltage in 0.4 kV bus in Scenario 2018/1.....	27
Figure 19. Reactive power window at 110 kV connection point of SSG from a) the measurement data and b) the simulation results.....	27
Figure 20. Reactive power window at 21 kV bus of SSG from a) the measurement data and b) the simulation results.....	27
Figure 21. Reactive power window at 110 kV side in Scenario 2018/2.....	28
Figure 22. Reactive power window at a) 110 kV b) 21 kV side for SSG in Scenario 2028/1.....	29
Figure 23. Voltages at 110 kV and 21 kV bus in Scenario 2028/2.....	29
Figure 24. Voltage at secondary transformers TR4272 and TR4318 400 V bus.....	30
Figure 25. Reactive power window for SSG with a) 1.5 MVAR and b) 1.75 MVAR shunt reactor in Scenario 2028/2.....	30
Figure 26. Reactive power window in Scenario 2028/3.....	31
Figure 27. Reactive power window in Scenario 2028/4.....	31
Figure 28. Reactive power window in Scenario 2028/5.....	31
Figure 29. Reactive power window in Scenario 2028/6.....	32
Figure 30. Reactive power window in Scenario 2028/7.....	32
Figure 31. Reactive power window at a) J06 Sulva and b) J07 Sundom feeder in Scenario 2028/8.....	33
Figure 32. Active and reactive power at J06 Sulva feeder in Scenario 2028/8.....	33
Figure 33. Active and reactive power at J07 Sundom feeder in Scenario 2028/8.....	33
Figure 34. Reactive power window in Scenario 2028/8.....	33
Figure 35. Reactive power window in Scenario 2028/9.....	34
Figure 36. Reactive power window in Scenario 2028/10.....	34
Figure 37. Reactive power window in Scenario 2035/0.....	35
Figure 38. Reactive power window in Scenario 2035/1.....	35
Figure 39. Reactive power window in Scenario 2035/2.....	36
Figure 40. Reactive power window in Scenario 2035/3.....	36
Figure 41. Reactive power window in Scenario 2035/4.....	37
Figure 42. Reactive power window at a) J06 Sulva and b) J07 Sundom feeder in Scenario 2035/4.....	37
Figure 43. Reactive power window in Scenario 2035/5.....	37
Figure 44. Reactive power window in Scenario 2035/5.....	38
Figure 45. Reactive power windows in Scenario 2018/1 offline when $T_s = 0.1$ s when a) (Q_h, P_h) and b) ($Q_{avg,h}, P_{avg,h}$) and the input data was step function.....	39
Figure 46. Reactive power windows in Scenario 2018/1 offline when $T_s = 0.1$ s when the input data was interpolated.....	39
Figure 47. Active and reactive power flows at HV/MV connection point in Scenario 2018/1 offline, the input data was step function.....	40
Figure 48. Voltage profiles at HV and at MV bus in Scenario 2018/1 offline.....	40
Figure 49. Voltage profiles at HV connection point in Scenario 2018/1 offline.....	40
Figure 50. Voltage profiles at MV connection points in Scenario 2018/1 offline.....	41

Figure 51. Reactive power window in Scenario 2018/2 offline when $T_s = 0.1$ s and a) input data was step function b) input data was interpolated.....	42
Figure 52. Reactive power window in Scenario 2018/2 offline when $T_s = 1$ s a) input data step function b) input data interpolated.....	42
Figure 53. Active and reactive power flows at HV/MV connection point in Scenario 2018/2 offline when $T_s = 0.1$ s.....	42
Figure 54. Active and reactive power of WT when input data was step type in Scenario 2018/2 offline when $T_s = 0.1$ s.....	43
Figure 55. Active and reactive power of WT when input data was interpolated in Scenario 2018/2 offline when $T_s = 0.1$ s.....	43
Figure 56. Reactive power window in Scenario 2028/1 offline when $T_s = 0.1$ s and input data was step function.....	43
Figure 57. Reactive power window in Scenario 2028/2 offline when $T_s = 0.1$ s, input data was a) step function, b) interpolated and when SR was voltage dependent.....	44
Figure 58. Reactive power window in Scenario 2028/3 offline when $T_s = 0.1$ s and input data was a) step function and b) interpolated.....	44
Figure 59. Reactive power window in Scenario 2028/4 offline when $T_s = 0.1$ s and input data was a) step function, b) interpolated. The shunt reactor Q was constant 1.75 MVar. The RPW controller was set up to the TSO limits.....	45
Figure 60. Reactive power window in Scenario 2028/4 offline when $T_s = 0.1$ s and input data was a) step function, b) interpolated. The shunt reactor was voltage dependent. The RPW controller was set up to the TSO limits.....	45
Figure 61. Reactive power window in Scenario 2028/4 offline when $T_s = 0.1$ s and input data was a) step function, b) interpolated. The shunt reactor Q was constant 1.75 MVar. The RPW controller was set up to the TSO limits +/- 50 kVar.....	45
Figure 62. Reactive power window in Scenario 2028/4 offline when $T_s = 0.1$ s and input data was a) step function, b) interpolated. The shunt reactor Q was voltage dependent. The RPW controller was set up to the TSO limits +/- 50 kVar.....	46
Figure 63. Reactive power window in Scenario 2028/4 offline when $T_s = 0.1$ s and input data interpolated. The shunt reactor Q was constant 1.75 MVar. The RPW controller was set up to the TSO limits ± 100 kVar.....	46
Figure 64. Reactive power of the WT converter in Scenario 2018/2 SIL, when $T_s = 1$ s, input data was step function and RPW control was set up to TSO limits.....	47
Figure 65. Reactive power of the WT converter in Scenario 2018/2 SIL, when $T_s = 0.1$ s, input data was step function and RPW control was set up to TSO limits.....	47
Figure 66. Reactive power of the WT converter in Scenario 2018/2 SIL, when $T_s = 0.1$ s, input data was interpolated and RPW control was set up to TSO limits.....	48
Figure 67. Reactive power window in Scenario 2018/2 SIL when $T_s = 0.1$ s and input data was a) step function, b) interpolated. The RPW controller was set up to the TSO limits.....	48
Figure 68. Reactive power of the WT converter in Scenario 2018/2 SIL, when $T_s = 1$ s, input data was step function and RPW control was set up to TSO limits ± 50 kVar.....	48
Figure 69. Reactive power of the WT converter in Scenario 2018/2 SIL, when $T_s = 1$ s, input data was interpolated and RPW control was set up to TSO limits ± 50 kVar.....	49
Figure 70. Reactive power window in Scenario 2018/2 SIL when $T_s = 1$ s and input data was a) step function, b) interpolated. The RPW controller was set up to the TSO limits ± 50 kVar.....	49
Figure 71. Reactive power of the WT converter in Scenario 2018/2 SIL, when $T_s = 0.1$ s, input data was step function and RPW control was set up to TSO limits ± 50 kVar.....	49
Figure 72. Reactive power of the WT converter in Scenario 2018/2 SIL, when $T_s = 0.1$ s, input data was interpolated and RPW control was set up to TSO limits ± 50 kVar.....	50
Figure 73. Reactive power window in Scenario 2018/2 SIL when $T_s = 0.1$ s and input data was a) step function, b) interpolated. The RPW controller was set up to the TSO limits ± 50 kVar.....	50
Figure 74. Reactive power of the WT converter in Scenario 2018/2 SIL, when when $T_s = 0.1$ s, input data was step function and RPW control was set up to TSO limits ± 100 kVar.....	50
Figure 75. Reactive power of the WT converter in Scenario 2018/2 SIL, when when $T_s = 0.1$ s, input data was interpolated and RPW control was set up to TSO limits ± 100 kVar.....	51
Figure 76. Test 1. Reactive power of the WT converter in Scenario 2018/2 CHIL (BBB), when $T_s = 1$ s, input data was step function and RPW control was set up to TSO limits ± 50 kVar.....	52
Figure 77. Test 2. Reactive power of the WT converter in Scenario 2018/2 CHIL(BBB), when $T_s = 0.1$ s, input data was step function and RPW control was set up to TSO limits ± 50 kVar.....	52
Figure 78. Test 3. Reactive power of the WT converter in Scenario 2018/2 CHIL (BBB), when $T_s = 0.1$ s, input	

data was step function and RPW control was set up to TSO limits..... 52

Figure 79. Test 4. Reactive power of the WT converter in Scenario 2018/2 CHIL (FPGA), when $T_s = 0.1$ s, input data was step function and RPW control was set up to TSO limits ± 50 kVAr..... 53

Figure 80. Test 5. Reactive power of the WT converter in Scenario 2018/2 CHIL (FPGA), when $T_s = 0.1$ s, input data was step function and RPW control was set up to TSO limits..... 53

Figure 81. Test 6. Reactive power of the WT converter in Scenario 2018/2 CHIL (FPGA), when $T_s = 1$ s, input data was step function and RPW control was set up to TSO limits..... 53

Figure 82. Test 7. Reactive power of the WT converter in Scenario 2028/2 CHIL (FPGA), when $T_s = 0.1$ s, input data was step function and RPW control was set up to TSO limits..... 54

Figure 83. Test 8. Reactive power of the WT converter in Scenario 2028/2 CHIL (FPGA), when $T_s = 0.1$ s, input data was step function and RPW control was set up to TSO limits ± 50 kVAr..... 54

Figure 84. Test 9. Reactive power of the WT converter in Scenario 2028/2 CHIL (FPGA), when $T_s = 0.1$ s, input data was step function and RPW control was set up to TSO limits ± 100 kVAr..... 54

Figure 85. Test 10. Reactive power of the WT converter in Scenario 2028/2 CHIL (BBB), when $T_s = 0.1$ s, input data was step function and RPW control was set up to TSO limits..... 55

Figure 86. Test 11. Reactive power of the WT converter in Scenario 2028/2 CHIL (BBB), when $T_s = 0.1$ s, input data was step function and RPW control was set up to TSO limits ± 50 kVAr..... 55

Figure 87. Test 12. Reactive power of the WT converter in Scenario 2028/2 CHIL (BBB), when $T_s = 0.1$ s, input data was step function and RPW control was set up to TSO limits ± 100 kVAr..... 55

Figure 88. Test 13. Reactive power of the WT converter in Scenario 2018/2 CHIL (BBB), when $T_s = 1$ s, input data was step function and RPW control was set up to TSO limits..... 56

Figure 89. GOOSE round trip latency for the BBB and FPGA. 57

Figure 90. BBB and FPGA GOOSE message processing time. 57

Figure 91. Reactive power of the WT converter in Scenario 2018/2 CHIL BBB and FPGA, when $T_s = 0.1$ s, input data was step function and RPW control was set up to TSO limits ± 50 kVAr, except QD1 limit to -0.2 MVar. 58

Figure 92. Reactive power of the WT converter in Scenario 2018/2 SIL and CHIL BBB, when $T_s = 0.1$ s, input data was step function and RPW control was set up to TSO limits ± 50 kVAr, except QD1 limit to -0.2 MVar. 58

Figure 93. Reactive power of the WT converter in Scenario 2018/2 SIL and CHIL FPGA, when $T_s = 0.1$ s, input data was step function and RPW control was set up to TSO limits ± 50 kVAr, except QD1 limit to -0.2 MVar. 59

Figure 94. Reactive power of the WT converter in Scenario 2018/2 BBB when $T_s = 0.1$ s and BBB when $T_s = 1$ s, input data was step function and RPW control was set up to TSO limits ± 50 kVAr, except QD1 limit to -0.2 MVar. 59

Figure 95. Reactive power of the WT converter in Scenario 2018/2 CHIL BBB and FPGA, when $T_s = 0.1$ s, input data was step function and RPW control was set up according to TSO limits except QD1 limit to 0. 59

Figure 96. Reactive power of the WT converter in Scenario 2018/2 CHIL BBB and FPGA as well as SIL, when $T_s = 0.1$ s, input data was step function and RPW control was set up according to TSO limits except QD1 limit to 0..... 60

Figure 97. Reactive power of the WT converter in Scenario 2018/2 CHIL BBB and FPGA, when $T_s = 0.1$ s, input data was interpolated and RPW control was set up according to TSO limits ± 50 kVAr..... 60

Figure 98. Reactive power of the WT converter in Scenario 2018/2 CHIL BBB and FPGA, when $T_s = 0.1$ s, input data was interpolated and RPW control was set up according to TSO limits, except QD1 limit to 0. 61

9.2 List of Tables

Table 1. State of the microgrid controller in IEEE and IEC standardization.....	9
Table 2. The simulation scenarios.....	19
Table 3. Line lengths of Sundom Smart Grid.....	28
Table 4. Forecasts for peak loads of Sundom Smart Grid.....	28
Table 5. Forecasts for PV units increase of Sundom Smart Grid.....	29
Table 6. Tests carried out as CHIL.....	51